THERMAL CONDUCTIVITY ENHANCEMENT IN MICRO- AND NANO-PARTICLE SUSPENSIONS

BY ANNA S. CHERKASOVA

A dissertation submitted to the

Graduate School—New Brunswick

Rutgers, The State University of New Jersey

in partial fulfillment of the requirements

for the degree of

Doctor of Philosophy

Graduate Program in Mechanical and Aerospace Engineering

Written under the direction of

Prof. Jerry W. Shan

and approved by

_____

_____

_____

_____

New Brunswick, New Jersey

October, 2009

ABSTRACT OF THE DISSERTATION

THERMAL CONDUCTIVITY ENHANCEMENT IN MICRO- AND NANO-PARTICLE SUSPENSIONS

by ANNA S. CHERKASOVA

Dissertation Director: Prof. Jerry W. Shan

It has been recognized that the addition of highly conductive particles can significantly increase the thermal conductivity of heat-transfer fluids. Particles in the micro- and nano-size range have attracted the most interest because of their enhanced stability against sedimentation and, as a result, reduction in potential for clogging a flow system. Additional interest has been drawn by recent reports of anomalous enhancements in thermal conductivity above predictions of classical theory for suspensions containing nano-particles. In this research we report on an experimental study of the effective thermal conductivity of suspensions containing micro- and nano-particles. First, we investigated the effect of the particle aspect ratio on heat transfer in fluids. Spherical and cylindrical silicon-carbide particles were dispersed in ethylene glycol, and multi-walled nanotubes were suspended in water with surfactant. To carry out a detailed analysis, size and geometry of the particles were determined from optical and transmission-electron-microscopy imaging. Provided the volume-averaged aspect ratio was used in theoretical calculations, the conductivity of the silicon carbide suspensions was found to be in excellent agreement with effective-medium theory. Experimental data on the thermal conductivity of multi-walled nanotubes dispersions could also be interpreted in terms of the aspect-ratio dependence predicted

by effective medium theory if the additional nanoscale effect of interfacial resistance was considered. The aspect ratio of dispersed particles was changed through further processing of both micro- and nano-fluids. As the result, the obtained thermal conductivities doubtlessly revealed that aspect ratio is a key factor affecting conductive heat transport in suspensions. For nanofluids, despite the promise of enhanced stability due to the nanoscale size of particles, particle agglomeration state can have a profound effect on the resulting thermal conductivity of the suspension. This was investigated by coupling thermal conductivity experiments with optical-absorbance and zeta-potential measurements of the stability of carbon nanotube-based nanofluids. An optimal surfactant-to-carbon nanotube mass ratio was found that resulted in both maximum thermal conductivity enhancement and suspension stability. Comparison of thermal conductivities for well-dispersed and agglomerated suspensions was carried out with the aid of ethanol de-stabilization. The experimental data indicated that only individualized nanotubes contribute appreciably to the thermal conductivity enhancement and, as a result, suspension stability is another essential parameter affecting the thermal conductivity of nanoparticle suspensions.

Acknowledgements

We thank A.E. Petersson for suggesting that we grind the silicon carbide suspensions with a ball mill, Y.W. Lu for allowing use of his microscope, L. D. Simon help in obtaining TEM images and the R.E. Riman group for allowing access to ZetaPALS Analyzer and other equipment. This work was supported by the National Science Foundation through grant CBET 0644719.

Table of Contents

List of Tables

List of Figures

List of Abbreviations

x, y, z	Cartesian coordinates
r, z, θ	spherical coordinates
ξ, ζ, ϕ	ellipsoidal coordinates
T	temperature
t	time
k	thermal conductivity of suspension
k_{p}	particle thermal conductivity
k_{b}	base fluid thermal conductivity
d	particle diameter
L	particle length
V	particle volume
N	particle number
b	spheroidal polar radius
c	spheroidal equatorial radius
e	eccentricity
n	shape factor
$f^{(i)}$	depolarization coefficient of a spheroid
a	aspect ratio of a spheroid
L_{P}	persistence length
L_{C}	contour length
L_{EE}	end-to-end length
R_{K}	Kapitza resistance
l_{K}	Kapitza length
g	gravity
A	absorbance
I	light intensity

Greek Letters

ϕ	volume fraction of particles
ρ_{p}	density of suspended phase
ρ_{b}	density of base fluid
δ	thermal conductivity ratio
μ	viscosity of base fluid
α	interfacial resistance coefficient

Subscripts

p	particle
b	base fluid
V	volume-weighted average
K	Kapitza
mean	mean value
peak	peak value
P	percolation
out	outside
in	inside

Chapter 1

Introduction

Heat-transfer fluids can exhibit significant increases in thermal conductivity with the addition of highly conductive particles. Recent attention has focused on micro- and nano- particle suspensions because of their enhanced stability against sedimentation, reduction in potential for clogging a flow system, as well as the tantalizing possibility of unexpected enhancements in thermal conductivity. The later has been spurred by reports of large increases in the thermal conductivity in very-low-volume fraction nanoparticle (up to 100 nm in size) suspensions. For instance, the effective thermal conductivity of an ethylene-glycol-based nanofluid containing copper nanoparticles with diameters less than 10 nm was reported to increase by up to 40% at 0.3% vol of dispersed particles [2]. Another example is silver nanoparticles in water and toluene [3], where thermal conductivity enhancement of 5-21% was observed at a loading of only 0.026% vol. The addition of less conductive aluminum oxide particles were reported to increase the resulting thermal conductivities of base fluids by up to 30% at particle volume fraction of Al_2O_3 of 5% [4], [5], 4% [6] or 3% [7]. In each case, the enhancements in thermal conductivity were reported to be greater than predicted by macroscopic theory for the given particle volume fraction and thermal conductivity.

Among nanoparticle suspensions, those containing carbon nanotubes (CNTs) have attracted some of the most interest. Discovered in 1991, carbon nanotubes have already entered the realm of practicality, finding use in the aerospace, automotive and telecommunications industries because of their interesting characteristics. Single-walled carbon nanotubes are 100 times stronger than steel at one-sixth the weight, and their

thermal conductivity is about 5-10 times greater than that of very conductive materials like aluminum or copper. Nanotubes can be electrical conductors or semiconductors depending on their crystal structure. Moreover, many physical properties of nanotubes, including their thermal conductivity, are expected to be highly anisotropic. Recent experiments have reported that carbon nanotubes greatly increase the thermal conductivity of fluids. For instance, Choi *et al.* reported a 2.5-fold increase in thermal conductivity of 1% vol of multi-walled nanotubes (MWNTs) in oil [8]. The thermal conductivity of poly α-olefin oil was enhanced by the factor of two for only 0.21% of MWNTs in the experiment by Yang *et al.* [9]. Early attempts to interpret these data in the light of existing theoretical models showed anomalous under-estimate of measured conductivities. The majority of theoretical models used at that time, such as Maxwell, Hamilton-Crosser, etc., did not take the aspect ratio of nanotubes into account. However, later theoretical work by Nan *et al.* [10] pointed out that, when the unusually high aspect ratio of CNTs is taken into account, the experimental data for carbon nanotube suspensions at least are within the bounds of effective medium theory (EMT). Even more, the unusually high aspect ratio of MWNTs can promote thermal conductivity enhancements that even exceed the reported "anomalous" thermal conductivity enhancements. However, at the nanoscale another important mechanism, the thermal resistance at the particle/liquid interface, must be accounted for in the case of nanofluids. Bringing the interfacial resistance into consideration can significantly lower the expected thermal conductivity enhancement.

All of this has stimulated new theoretical and computational analysis [11, 12, 13, 14] of the effective thermal conductivity of nanoparticle dispersions. Brownian motion, interparticle clustering, ballistic phonon transport have been considered as possible mechanisms responsible for conductive-heat-transfer amplifications in nanofluids.

The objective of this work is an experimental exploration of the thermal conductivity of micro- and nano-particle dispersions. The goals of the proposed work are threefold:

1) Compare thermal conductivity increase in suspensions containing micro- and

nano-sized particles of different shape with effective medium theory. As the first step, the conductivity of silicon carbide (SiC) particles is measured and compared with classical theory. Particle size was initially chosen to be in the micron range to avoid effects which are scale-dependant, such as interfacial resistance or Brownian motion. After that, we will analyze thermal conductivity of nano-fluids containing multi-walled carbon nanotubes. A careful comparison with theory is made including the effect of interfacial resistance.

2) Investigate the aspect-ratio effect on the thermal conductivity of suspensions. In this set of experiments, only the effect of particle aspect ratio on heat transfer in composite materials will be investigated. In order to do this, the aspect ratio of cylindrical SiC particles was directly varying through milling. For CNTs we reduce their length through intensive sonication. Measuring the particle aspect ratio for each sample directly from the optical and TEM micrographs allows us to carry out a detailed comparison with effective medium theory. Some recent data in the literature on the thermal conductivity of nanotube suspensions is also analyzed in light of the aspect-ratio effect predicted by EMT.

3) Study particle agglomeration effect on the thermal conductivity of nanoparticle suspensions. It turns out that the preparation of nano-suspension with large, stable fraction of individualized tubes/particles is an extremely complicated task. It is possible though to analyze the level of particle aggregation quantitatively by measuring either the zeta-potential or optical absorbance of the suspension. In some cases we can vary the degree of agglomeration, especially in water-based solutions. We chose surfactant stabilization to control the dispersion characteristics of the nanofluids. We evaluate the aggregation state of the aqueous MWNTs suspensions and its effect on thermal conductivity. An optimal surfactant concentration resulting in maximum thermal conductivity increase is found. As the final step, we de-stabilize previously stable nanofluids with ethanol addition and correlate the thermal conductivity of these modified nanofluids with optical absorbance measurements of their aggregation state.

Chapter 2

Modeling of the Thermal Conductivity of Composite Materials

2.1 Spherical Particle in Infinite Medium

Theoretical modeling of the effective conductivity of a composite material dates back to Maxwell [15], who derived the expression for the electrical conductivity of a two-component mixture. However, all the considerations could be easily applied to the thermal conductivity as well, since the governing equations are similar. Let us consider a composite suspension made of homogeneous spheres evenly dispersed in a matrix liquid with heat conduction as the only heat flow mechanism. Assuming no interaction between particles we can solve Laplace equation for the simplest configuration when the only sphere of radius R is immersed in infinite medium and subjected to the uniform heat flux, as shown in Fig. 2.1. In this case, the spatial distribution for temperature outside and inside the sphere is [16]:

$$T_{\text{out}} = Ar(1 + \frac{B}{r^3})\cos\theta = Az(1 + \frac{B}{r^3}), \tag{2.1a}$$

$$T_{\text{in}} = Cr\cos\theta = Cz. \tag{2.1b}$$

The first term in the expression for T_{out} denotes the linear temperature change along the direction of heat flux. The second term is a fluctuation or disturbance caused by the presence of a sphere and this fluctuation vanishes as $r \to \infty$. Inside the sphere temperature is linear along the *z*-axis. The following boundary conditions have to be applied at the surface of a sphere in order to to find the unknown coefficients *A* and *B*:

$$T_{\text{out}} = T_{\text{in}}, \tag{2.2a}$$

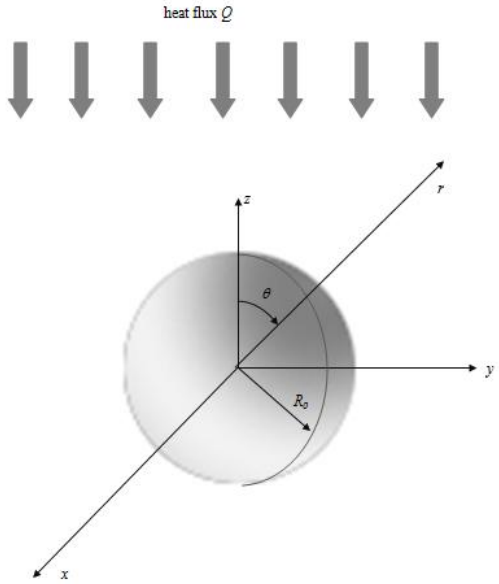

Figure 2.1: Spherical particle in infinite medium subjected to a uniform heat flux Q

$$-k_{\mathrm{b}}\frac{\partial T_{\mathrm{out}}}{\partial r} = -k_{\mathrm{p}}\frac{\partial T_{\mathrm{in}}}{\partial r}, \tag{2.2b}$$

where k_{b} and k_{p} are thermal conductivities of base medium and particle material correspondingly. The first boundary condition means no interfacial resistance exists between the particle and the fluid, or the interface is perfect. The second one indicates that no heat accumulation takes place at the surface. Solving Eqs. 2.1 together with their boundary conditions we obtain coefficients as follows

$$B = \frac{R^3(1-\delta)}{2+\delta} \tag{2.3}$$

and

$$C = \frac{3A}{2+\delta}. \tag{2.4}$$

Here a dimensionless parameter, δ, is defined as ratio of thermal conductivities of particle and base medium

$$\delta = k_{\mathrm{p}}/k_{\mathrm{b}}. \tag{2.5}$$

2.2 Maxwell Model

Let us briefly review the approach for obtaining formula for thermal conductivity of composite materials containing spherical inclusions following Maxwell. First, we note that the analytical solution of the Laplace equation for a single sphere, placed in a infinite medium and subjected to a uniform heat flux, exists as given by Eqs. 2.1. If boundary conditions on the surface of a sphere are given in a form of continuity of temperature and normal component of a heat flux, the temperature distribution is known at any point inside and outside the sphere. Let us now consider N homogeneous spheres, each of radius R_0, suspended in an infinite medium. If the distances between the spheres are large, we assume no interaction between them, *i.e.* each sphere can be treated as a single sphere in infinite medium. The temperature at some distance far away from the particles is given by:

$$T = \sum_{i=1}^{N} Az(1 + n\frac{R_0^3}{r_i^3}\frac{1 - k_\mathrm{p}/k_\mathrm{b}}{2 + k_\mathrm{p}/k_\mathrm{b}}) \cong Az(1 + n\frac{R_0^3}{r^3}\frac{1 - k_\mathrm{p}/k_\mathrm{b}}{2 + k_\mathrm{p}/k_\mathrm{b}}), \tag{2.6}$$

Let us suppose that all spherical particles are positioned within one large imaginary sphere of radius R_1. Assuming that effective thermal conductivity of material of the sphere is k, temperature outside the sphere is given by equation similar to Eq. 2.6:

$$T = Az(1 + \frac{R_1^3}{r^3}\frac{1 - k/k_\mathrm{b}}{2 + k/k_\mathrm{b}}). \tag{2.7}$$

Now, the spherical volume, that confines all particles suspended in a liquid, can be replaced with one large sphere. This sphere is thermally *equivalent* to the suspension only if temperatures given by Eq. 2.6 and Eq. 2.7 are the same:

$$\sum_{i=1}^{N}(1 + N\frac{R_0^3}{r_i^3}\frac{1 - k_\mathrm{p}/k_\mathrm{b}}{2 + k_\mathrm{p}/k_\mathrm{b}}) \cong (1 + N\frac{R_0^3}{r^3}\frac{1 - k_\mathrm{p}/k_\mathrm{b}}{2 + k_\mathrm{p}/k_\mathrm{b}}) = (1 + \frac{R_1^3}{r^3}\frac{1 - k/k_\mathrm{b}}{2 + k/k_\mathrm{b}}) \tag{2.8}$$

Solving the Eq. 2.8 for the effective thermal conductivity of suspension, we obtain the following formula for k:

$$k = k_{\mathrm{b}}(1 + \frac{3\phi(\delta - 1)}{\delta + 2 - \phi(\delta - 1)}). \tag{2.9}$$

Here, ϕ is a volume concentration of particles, defined as $\phi = NR_0^3/R_1^3$.

The above equation, called the Maxwell equation for thermal conductivity of composite material, is derived under the following assumptions:

1) the suspended particles are spherical;

2) the particles are non-interacting;

3) the interfacial resistance between the liquid and solid phases is negligible.

The Maxwell model for thermal conductivity of composites has some limitations. Above all, the volume fraction of suspended in liquid particles has to small enough in order to assume no interaction between them. However, there is considerable experimental evidence for the validity of the Maxwell model for thermal conductivities of non-nanoscale particulate suspensions. Equation 2.9 agrees well with experimental data for spherical-particle suspensions with volume fraction less than approximately 10% - 20% when the conductivity ratio is high, *i.e.* $\delta = k_{\mathrm{p}}/k_{\mathrm{b}} >> 1$ [17]. At higher volume fractions, the particles can not be considered to be isolated from each other, or they even can form a percolated network. For spherical particles, the percolation threshold concentration is around 16% vol, even though percolation due to the fractal formation can start earlier [18]. In this case the initial assumptions of the Maxwell model fail to describe mechanism of heat transfer in composite material. Our experiments are capped by the volume fractions far below the threshold concentration to ensure evenly dispersed suspensions with no percolated network for heat to flow along.

2.3 Fricke Model for Spheroidal Inclusions

A model for the effective thermal conductivity of a dilute suspension of randomly oriented spheroidal particles was developed by Fricke [19], using a method similar to

Maxwell's approach. Let us consider a prolate spheroid oriented in liquid so that its axis of rotational symmetry is along the z-axis. For convenience we introduce prolate spheroidal coordinates ξ and ζ. The relations between Cartesian x, y and z and spheroidal coordinates are expressed as

$$x = \pm\sqrt{\frac{(\xi + b^2)(\zeta + b^2)}{b^2 - c^2}}\sin\phi,$$

$$y = \pm\sqrt{\frac{(\xi + b^2)(\zeta + b^2)}{b^2 - c^2}}\cos\phi,$$

$$z = \pm\sqrt{\frac{(\xi + c^2)(\zeta + c^2)}{c^2 - b^2}},$$

where $\xi \geq -b^2$, $-b^2 \geq \zeta \geq -c^2$ and $0 \leq \phi < 2\pi$.

The surfaces of a constant ξ are confocal spheroids, and $\xi = 0$ corresponds to the surface of the particle. After solving Laplace equation in spheroidal coordinates, the exact solution for temperature distribution inside and outside the spheroid can be obtained. The following derivation applies to the case of prolate spheroids, where it is assumed that the spheroid has aspect ratio $a = c/b$, where c and b are spheroidal polar and equatorial radii. The solution of the heat-transfer equation for temperature in the case of a spheroidal particle suspended in infinite medium has a following form:

$$T = Az(1 + \frac{cb^2}{2}\frac{1 - \delta}{f^{(i)}(\delta - 1) + 1}F(\xi)), \tag{2.10}$$

Here F is a function of ξ only and it is defined by

$$F(\xi) = \int_{\xi}^{\infty} \frac{ds}{(s + b^2)\sqrt[3]{(s + c^2)}}. \tag{2.11}$$

If the spheroid is aligned along the heat flux with its longest axis, $i = z$ and

$$f^{(z)} = \frac{1 - e^2}{e^3}(\tanh^{-1} e - e), \tag{2.12}$$

if the spheroid is perpendicular to the field, $i = x$ and

$$f^{(x)} = (1 - f^{(z)})/2. \tag{2.13}$$

Coefficients $f^{(z)}$ and $f^{(x)}$ are so-called depolarization factors, which depend on the geometry of the particle through its eccentricity e, which is always a non-negative number less then 1:

$$e = \sqrt{1 - (\frac{b}{c})^2}.$$

Following the Fricke approach further, we assume uniformly dispersed and oriented spheroidal particles suspended in a liquid. We write the resulting expression for thermal conductivity of such suspension has a following form:

$$k = k_{\mathrm{b}}(1 + \frac{n\phi(\delta - 1)}{(n-1) + \delta - \phi(\delta - 1)}). \tag{2.14}$$

Here, n is the dimensionless shape factor given by

$$n = \frac{\beta\delta - \beta}{\delta - 1 - \beta}, \tag{2.15}$$

where

$$\beta = \frac{1}{3}(\delta - 1)\left(\frac{2}{1 + (\delta - 1)f^{(x)}} + \frac{1}{1 + (\delta - 1)f^{(z)}}\right). \tag{2.16}$$

For spheres, all of the depolarization factors are equal to each other, resulting in n=3. In this case Eq. 2.14 coincides with the Maxwell formula (Eq. 2.9). For large-aspect-ratio particles, such as nanotubes, the Fricke prediction for effective thermal conductivity can greatly exceed that of the Maxwell model as seen in Fig. 2.2. Experimental evidence for a quantitative aspect-ratio effect on the thermal conductivity, particularly in fluid suspensions, is limited, however. The largest amount of experimental research for suspensions containing high-aspect-ratio filler is attributed to nanofluids. However, in general, the particle geometry and aggregation state are not well characterized in most nanofluid experiments. Also, the thermal conductivity of nanoparticle and nanotube suspension can be affected by some scale-dependent mechanisms that enter into consideration only at smaller scales and not taken into account in conventional

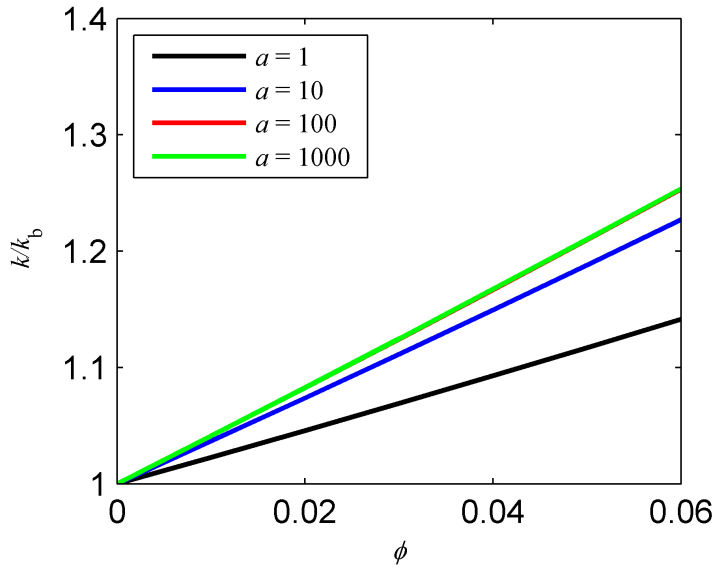

(a) δ=10

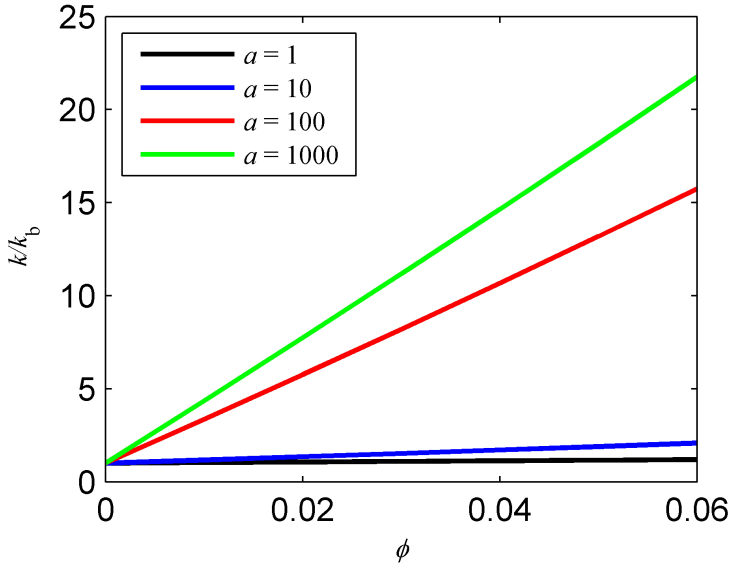

(b) δ=1000

Figure 2.2: Calculated thermal conductivity enhancements in suspensions

macroscopic-scale models like Maxwell's or Fricke's. Among these effects there is interfacial resistance at solid-liquid interfaces, which becomes increasingly important due to the larger number of interfaces for a given volume fraction of solid content as the particle size decreases. For example, for spherical particles, the particle surface area per unit volume scales as $1/r$ for a fixed particle concentration.

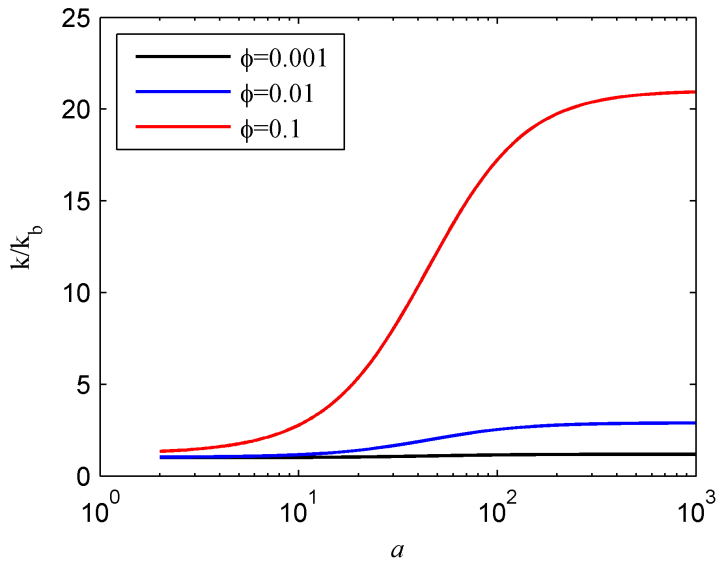

Figure 2.3: Calculated thermal conductivity enhancements for varying aspect ratio of dispersed particles

2.4 Conductivity Ratio, δ

Among other parameters affecting the thermal conductivity of composite materials, the thermal conductivities of both the dispersed and dispersing media play an important role. The base fluid thermal conductivity is usually well-known, or can be measured directly. However, the thermal conductivity of dispersed particles is not always known exactly, especially in the case of nanoparticles, when it can be quite different from the thermal conductivity of bulk material. Nevertheless, a rough estimate is sometimes enough to use in Eqs. 2.9 and 2.14. As expected, thermal conductivity

enhancement is increasing with the increase of the ratio of conductivity of dispersed medium over base fluid, δ. However, for suspension of spherical particles, k saturates at some δ, as can be seen from Eq. 2.9. If $\delta \to \infty$, the effective thermal conductivity of the suspension k approaches its limit at:

$$k = k_{\mathrm{b}}(1 + \frac{3\phi}{1-\phi}). \tag{2.17}$$

It can be seen from Fig. 2.4 that after $\delta = 100$ the thermal conductivity of the suspension is completely insensitive with regards of δ. This means that the thermal conductivity enhancement due to increase in thermal conductivity of dispersed material, while other parameters are fixed, is negligible assuming that δ is high enough. In practice, this is somewhat true for nanofluids containing highly-conductive additives, such as copper ($k_{\mathrm{p}} = 400$ W/mK), silicon carbide ($k_{\mathrm{p}} \approx 400$ W/mK), etc. Thermal conductivity of regular fluids ranges, for instance, from 0.18 W/mK for ethanol up to 0.6 W/mK for water, giving a conductivity ratio well above 100.

In the case of non-spherical particles, this effect depends on aspect ratio of dispersed particles a lot. It can be clearly seen in Fig. 2.4 that saturation occurs at $\delta \approx 10^3$ for suspensions containing dispersed spheroidal particles with $a = 35$, and at $\delta \approx 5 \times 10^3$ when $a = 100$. For longer particles with $a > 500$, k never saturates and is proportional to the conductivity ratio.

2.5 Particle Aspect Ratio Distribution

As was mentioned above, both Maxwell and Fricke models were derived under assumption that particle size/aspect ratio is fixed. It is not clear how to calculate effective thermal conductivity of suspension containing spheroidal particles if aspect ratio distribution is not a Delta-function. There are numerous possible characteristic dimensions associated with the particle aspect ratio distributions, *e.g.* the mean aspect ratio a_{mean}, most probable aspect ratio a_{peak} or the median aspect ratio. However, we can show that the volume-weighted aspect ratio is the correct measure to use. Following Frickes approach, we obtain a modified formula for the parameter β:

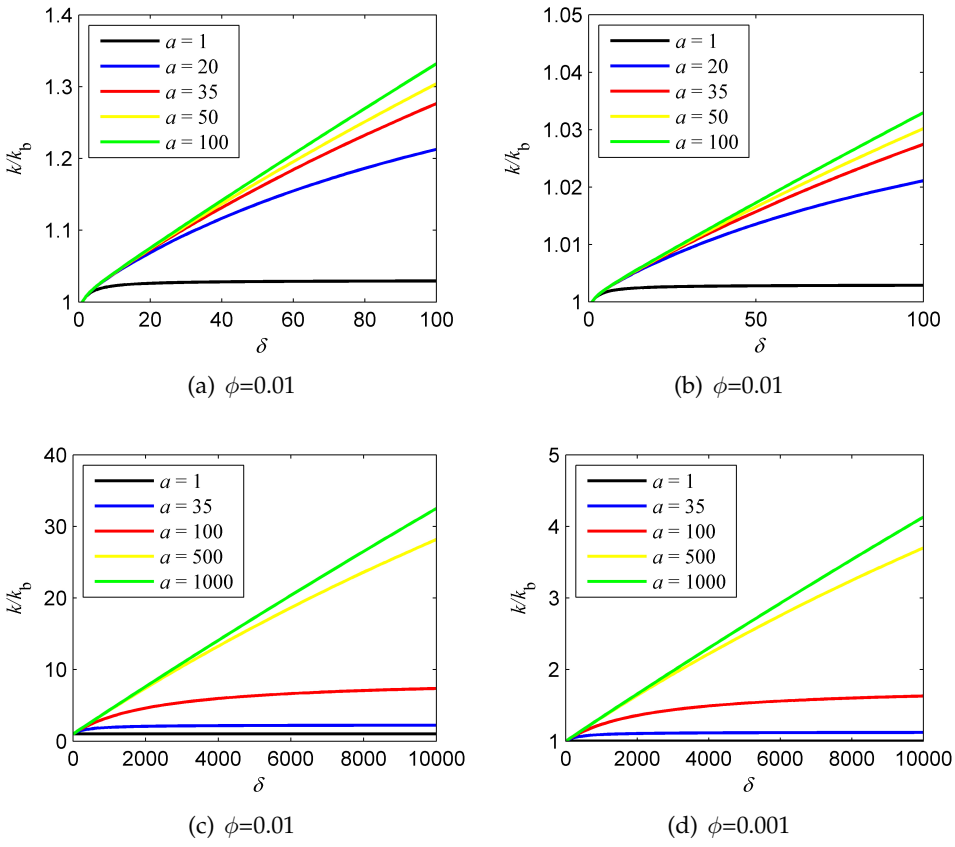

(a) ϕ=0.01 (b) ϕ=0.01

(c) ϕ=0.01 (d) ϕ=0.001

Figure 2.4: Conductivities ratio, δ, effect on calculated thermal conductivity of suspensions for different aspect ratio of dispersed particles

$$\beta = \frac{1}{3}(\delta - 1)\frac{\sum_1^N V_i \left(\frac{2}{1+(\delta-1)f^{(x)}} + \frac{1}{1+(\delta-1)f^{(z)}}\right)}{\sum_1^N V_i}, \tag{2.18}$$

where the functions $f^{(x)}$ and $f^{(z)}$ are given by Eqs. 2.13 and 2.12 for every particle.

The outer summation in Eq. 2.18 can be replaced by an integral if an aspect ratio distribution is given. Sample calculations for a suspension of volume fraction of 2.5% are shown in Fig. 2.5. Thermal conductivities of the suspended and suspending media are taken as 360 W/mK and 0.25 W/mK, respectively. The particles were assumed to have a log-normal aspect-ratio distribution with logarithm standard deviations of either 0.5 or 2. Calculations based on log-normal aspect ratio distribution are compared with data obtained using the peak (a_{peak}) , mean (a_{mean}) and volume-weighted (a_{V}) aspect ratios in the Fricke equation.

It can be seen that the conductivity calculated using the volume-weighted aspect ratio, given by

$$a_{\mathrm{V}} = \frac{\sum_1^N a_i V_i}{\sum_1^N V_i}, \tag{2.19}$$

is most consistent with the full calculation. This result can be attributed to the fact that the thermal-conductivity contribution of the particles having a particular aspect ratio should depend on the total volume of such particles rather than on their number. Also, it should be noted that the distribution width affects the calculated thermal conductivity of the suspension; when σ increases, the thermal conductivity increases because the fraction of long particles, which contribute more to total thermal conductivity enhancement, is higher even though the peak aspect ratio can stay the same. For a monodisperse suspension (Delta-function distribution of particle aspect ratios), all three characteristic aspect ratios, (a_{peak}), (a_{mean}) and (a_{V}), are the same and the thermal conductivity calculated using the distribution coincides with that predicted by Eq. 2.14. We note that, though these calculations were made for the Fricke model, which assumes no interfacial resistance on the surface of the particle, the same approach can be applied to Nan's more general model, discussed later.

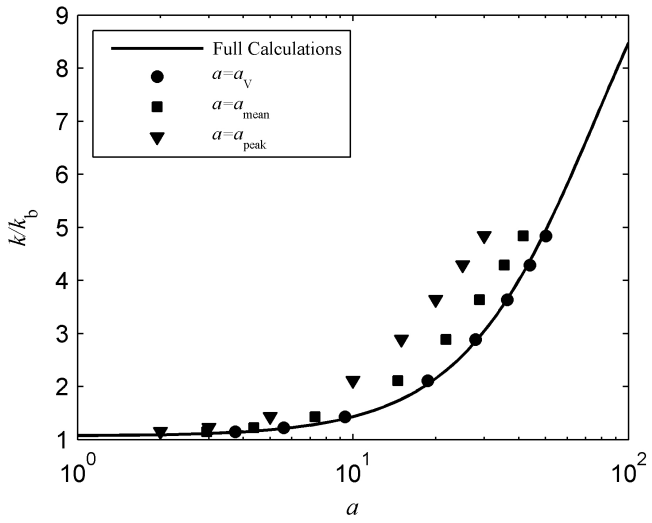

(a) $\sigma = 0.5$

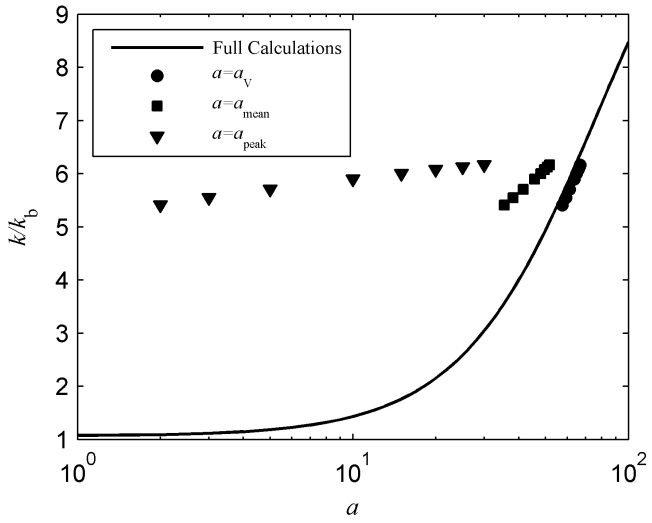

(b) $\sigma = 2.0$

Figure 2.5: Calculated thermal conductivity of a 2.5% SiC-in-oil suspension with log-normal aspect ratio distribution

2.6 Thermally Interacting Particles

As was discussed above, models for calculating thermal conductivity in suspensions of both spherical and spheroidal particles were derived under the assumption of thermally non-interacting inclusions. This assumption breaks when particles directly contact with each other, forming a percolated network, conducting for heat flow. However, particles can begin to interact with each other thermally in suspension at concentrations even below the critical percolation volume fraction ϕ_{P}. The mechanism describing this type of interaction arise from the fact that, at some concentration, the initial approach of solving the Laplace equation for a single particle immersed in infinite medium becomes invalid. In this high-concentration case, every particle is affected by the disturbance of temperature field caused by the presence of all other particles. An approach which takes into account not the influence of all, but only neighborhood spheres, was introduced by Bruggeman [20]. The integration-embedding principle consists of consecutive iterations in volume fractions, with the effect of particles added before is taken into account at every step. The Bruggeman iterative method allows finding thermal conductivity of the suspension numerically. Numerical solution comes from a linearized Maxwell equation:

$$k = k_{\mathrm{b}}(1 + \frac{3\phi(\delta - 1)}{\delta + 2}). \tag{2.20}$$

If we add small amount of the same particles to this suspension, then the effective thermal conductivity is given by the following equation:

$$k(\phi + d\phi) = k(\phi)(1 + \frac{3d\phi(k_{\mathrm{p}} - k(\phi))}{k_{\mathrm{p}} + 2k(\phi)}). \tag{2.21}$$

The above equation can be integrated in a form:

$$(\frac{k - k_{\mathrm{p}}}{k_{\mathrm{b}} - k_{\mathrm{p}}})(k/k_{\mathrm{b}})^{1/3} = 1 - \phi. \tag{2.22}$$

According to the Bruggeman approach, thermal interaction between spheres affect the resulting conductivity of composite fluid at volume fractions above ∼15% [21], which is also comparable with formation of percolation paths in the suspension. It can be also seen from Fig 2.6, that adjustment for inter-particle interaction has less effect on k as δ increases. This comes from the fact that we change the base fluid, and conductivity ratio therefore, with iterations. At the same time, as δ increases it has less or no effect on thermal conductivity enhancement, as was shown before.

A similar approach can be applied to the case of spheroidal inclusions as well. In this case, no direct integration of the iterative equation is possible, so we need to iterate the full, non-linearized, equation for the thermal conductivity of a suspension containing spheroidal particles:

$$k(\phi + d\phi) = k(\phi)(1 + \frac{nd\phi(k_{\mathrm{p}} - k(\phi))}{(n-1)k_(\phi) + k_{\mathrm{p}} - d\phi(k_{\mathrm{p}} - k(\phi))}). \tag{2.23}$$

Figure 2.6 shows a comparison of the thermal conductivities predicted by Maxwell, Fricke and Bruggeman. It is clearly seen that for spherical particles that the thermal conductivity enhancements match for volume concentrations up to ∼5-15% depending on δ. The difference in calculated thermal conductivities is vanishing as δ increases. This result comes from the fact that the presence of other thermally "visible" particles in suspension effectively increase the base fluid thermal conductivity for any individual particle immersed in the suspension. However, as was discussed above, δ has no effect on k_{b} once it is above ≈100 depending on particle concentration. In this limiting case Maxwell and Bruggeman models provide the same thermal conductivity enhancement given by Eq. 2.17. As the aspect ratio of dispersed particles increases, the thermal conductivity ratio δ has more effect on suspension conductivity k, resulting in a difference between Fricke predictions and conductivities calculated with the interacting method. As the particle aspect ratio or δ increases, the difference in thermal conductivity given by these two methods occurs earlier with respect to particle concentration for suspension containing ellipsoidal inclusions. However, even though the thermal particle interaction becomes more and more important as the particle aspect

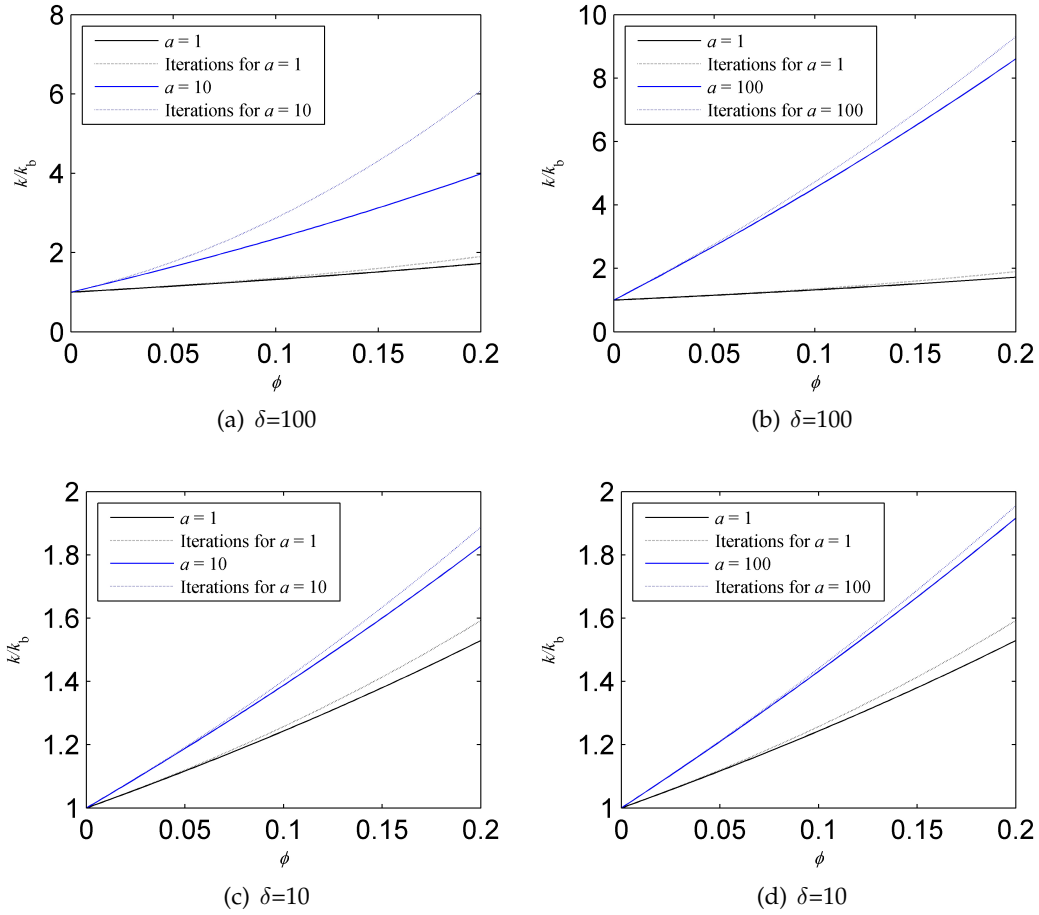

(a) δ=100 (b) δ=100

(c) δ=10 (d) δ=10

Figure 2.6: Comparison of calculated thermal conductivity enhancements for suspension containing non-interactive particles and using the Bruggeman approach

ratio increases, its effect on the suspension thermal conductivity is still negligible at low fraction on dispersed particles. In our experiments, the maximum particle volume fractions used were 5% for SiC and 1% for MWNTs, still below the threshold for thermally interacting suspensions.

2.7 Interfacial Resistance

In the case of energy transport, continuum theory assumes continuity in both temperature and energy, or heat, flux across the interface. This assumption works very well at the macroscopic scale, but breaks down as the problem's characteristic length decreases. In this case temperature is not conserved across the interface of two phases. A phenomenological approach to describe a discontinuity in temperature at liquid/solid interface dates back to Kapitza [22], who suggested that temperature at the interface undergoes a change proportional to the normal component of the heat flux through the interface:

$$T_{\text{out}} - T_{\text{in}} = -R_{\text{K}} \times q_{\text{interface}}. \tag{2.24}$$

Here, R_{K} is Kapitza, or thermal contact, resistance.

The Kapitza resistance appeared first and has been studied intensively in the context of liquid helium physics, but it exists on every interface between two phases. The magnitude of the resistance, R_{K} depends on many parameters such as thermal properties of materials in contact along with their physical properties. An important practical question is how this thermal contact resistance affects thermal conductivity of composite material. An obvious answer is that Kapitza resistance can lower nanofluid thermal conductivity significantly as interface density increases. To investigate this effect we follow the Maxwell approach for obtaining the thermal conductivity of suspensions. Instead of temperature continuity at the liquid/solid interface, we use Eq. 2.24 as boundary condition. This leads to the following equation for thermal conductivity of a composite containing spherical particles:

$$k = k_{\mathrm{b}}(1 - 3\phi \frac{k_{\mathrm{b}} + \frac{k_{\mathrm{p}}}{1+\frac{k_{\mathrm{p}}R_{\mathrm{K}}}{R}}}{2k_{\mathrm{b}} + \frac{k_{\mathrm{p}}}{1+\frac{k_{\mathrm{p}}R_{\mathrm{K}}}{r}} + \phi(k_{\mathrm{b}} - \frac{k_{\mathrm{p}}}{1+\frac{k_{\mathrm{p}}R_{\mathrm{K}}}{R}})}), \tag{2.25}$$

which converts to the regular Maxwell formula with k_{p} replaced by an effective thermal conductivity of dispersed phase $k_{\mathrm{p}}^{(\mathrm{e})}$ given by

$$k_{\mathrm{p}}^{(\mathrm{e})} = \frac{k_{\mathrm{p}}}{1 + \frac{k_{\mathrm{p}}R_{\mathrm{K}}}{R}}. \tag{2.26}$$

2.8 Nan's Effective Medium Theory

A model for the thermal conductivity of suspensions of randomly oriented ellipsoidal inclusions was also generalized to include the effect of interfacial resistance in the form of an effective medium theory (EMT) by Nan [10]. Nan showed that for a dilute suspension of randomly oriented, spheroidal particles with radius b (along the short axis for a prolate spheroid) and interfacial (Kapitza) resistance R_{K}, the thermal conductivity is given by:

$$k = k_{\mathrm{b}} \left(1 + \frac{\phi(2\beta_x + \beta_z)}{3 - \phi(2\beta_x f^x + \beta_z f^z)} \right), \tag{2.27}$$

where

$$\beta_{ii} = \frac{k_{ii} - k_{\mathrm{b}}}{k_{\mathrm{b}} + f^i(k_{ii} - k_{\mathrm{b}})} \tag{2.28}$$

$$k_{ii} = k_{\mathrm{p}} + k_{\mathrm{b}}(1 - f^{(i)})(2 + \frac{1}{a})\alpha. \tag{2.29}$$

Here, α is a dimensionless measure of the interfacial resistance, defined as

$$\alpha = \frac{R_{\mathrm{K}}k_{\mathrm{b}}}{b}, \tag{2.30}$$

with α=0 denoting a perfect interface having no temperature jump.

Most of experimental data on heat transfer in nanofluids corresponds to the suspensions containing spherical particles. Although a number of experiments on thermal conductivity of CNT nanofluids have been reported, there is no systematic study on particle aspect ratio effect on thermal conductivity in suspensions. Experimental measurements have been made in composite materials consisting of slightly prolate (a=2) or oblate (a=0.5) diamond particles in zinc sulfide (ZnS) [23]; the measured conductivities were later found to be in good agreement with EMT. For fluid suspensions, Xie *et al*. measured the thermal conductivity of spherical and cylindrical silicon carbide (SiC) particles dispersed in water and ethylene glycol (EG) [1]. Measurements were conducted for suspensions with particles volume fraction up to 5% at 4 ^{o}C. Thermal conductivity for suspension containing spherical particles with average diameter 900 nm is predicted very well by Maxwell model. Substantially higher thermal conductivity enhancements were found for the cylindrical particles than the spherical ones. This result is qualitatively consistent with EMT, but, unfortunately, no precise information was given about aspect ratio of the SiC whiskers. Yang and Han [24] studied the thermal conductivity of bismuth telluride (Bi_2Te_3) nanorods in perfluoro-*n*-hexane (FC-72) and in hexadecane oil. The nanorods had an average diameter of 20 nm and the average length of 170 nm, giving an aspect ratio of 8.5. Measurements conducted in a wide range of temperatures for suspensions containing 0.8% vol of particles, showed higher thermal conductivities than predicted by the Maxwell theory for spherical particles, and were roughly consistent with EMT calculations. A slight enhancement in thermal conductivity above EMT predictions was attributed to the Brownian motion of the nanoparticles. No attempt was made to vary the aspect ratio, degree of aggregation, or orientation of the nanorods. In the following, we first report on a careful comparison of Fricke/EMT predictions with experimental data on micro-sized SiC particles, as well as MWNTs suspensions in water. A systematic study is made of the effect of particles aspect ratio in both micro- and nano-suspensions, and the effect of particle aggregation on the thermal conductivity of nanotube suspension is also investigated.

Chapter 3

Methods and Materials

3.1 Experiment Setup

Thermal conductivity of micro- and nano-suspensions was measured using a transient hot-wire apparatus (KD-2 Thermal Properties Analyzer, Decagon Devices, Inc.). The hot-wire measures the thermal conductivity, k, and thermal resistivity from the rate of temperature increase of the probe for a constant heating rate. The needle serves as both thermometer and a heating source in this case. The classical solution of the heat transfer equation for a thin probe, or wire, immersed in an infinite medium is utilized for computing heat conductivity from the probe heating rate:

$$k = \frac{Q}{4\pi \frac{dT}{d(lnt)}} \tag{3.1}$$

where Q is the heating rate per unit length of the wire, T is the measured temperature and t is time.

In the KD2, the hot wire is encapsulated in a needle to avoid problems which can arise while measuring the thermal conductivity of electrically conductive fluids. As shown in Fig. 3.1, literature values for thermal conductivity of ethylene glycol, mineral oil, ethanol and glycerin [25] were reproduced with error less then 5%, which is declared accuracy of KD2. The KD2 conforms to ASTM D5334 and IEEE 442-1981 standards for determining thermal conductivity.

All measurements were conducted at a constant temperature, which was maintained stable with the aid of temperature-controlled recirculating bath as shown in Fig. 3.2. Temperature deviations did not exceed 0.5 ^{o}C for microfluid experiment and 0.3 ^{o}C for nanofluids. Maintaining steady temperature is essential for the hot-wire

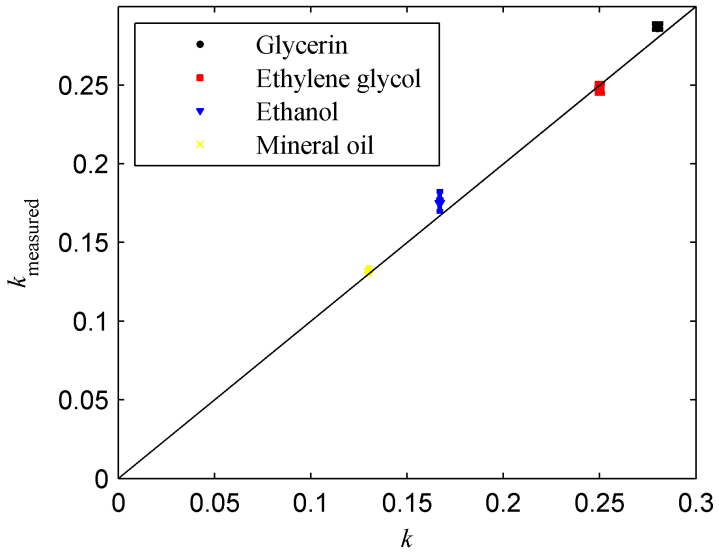

Figure 3.1: KD2 calibration

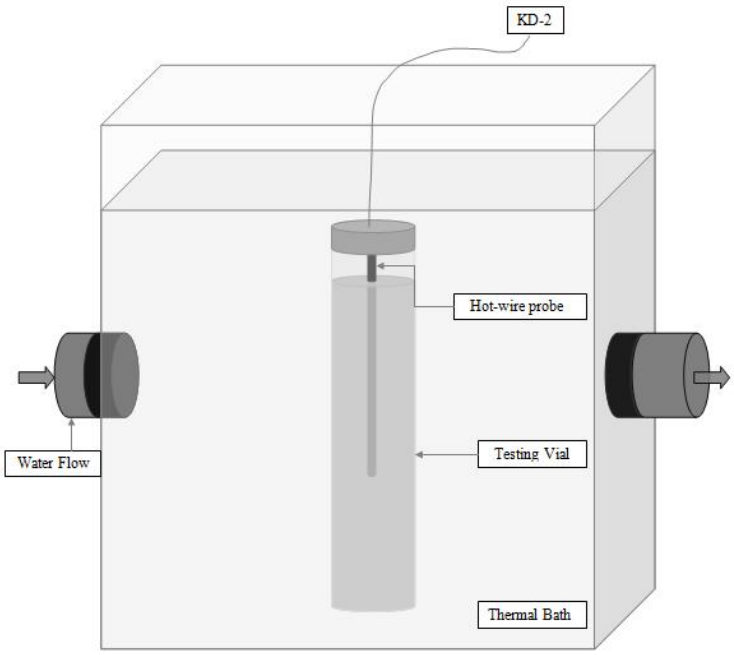

Figure 3.2: Experimental setup for thermal conductivity measurements

method because effects caused by convection can significantly distort temperature field around the probe and corrupt the measurements. In the present experimental study the temperature varied by the maximum of 0.2-0.5 ^{o}C from the one sample to another, but did not exceed 0.1 ^{o}C for a single measurement.

We started our experimental investigation with heat transfer analysis in microfluids. In the first set of measurements, two types of micron-size silicon carbide particles (Alfa Aesar Corp., Ward Hill, MA) were dispersed in ethylene glycol:

1) Spherical particles (-325 mesh, 99% metals basis, Item #43332, Lot #K14R005) with diameters less then 40 microns;

2) Whiskers 1.5 microns in diameter and nominally 18 microns in length (99% metals basis, Item #38787, Lot #D03S014).

As the second part of this study, we conducted experiments on suspensions containing MWNTs (short, Stock #1238YJS, Lot #1238-070108) with with nominal lengths of 0.5 - 2 microns and outer diameters of 30-50 nm, as reported by the manufacturer (Nanostructured and Amorphous Materials, Inc., TX).

Micro-particle suspensions with volume concentration of solid up to 5% were obtained by mixing SiC particles with ethylene glycol (Stock #8673122, Mc-Master Carr, Atlanta, GA). After being mechanically stirred vigorously, all samples were further homogenized with the aid of bath sonicator (RTE-100 by NESLAB) for 30 minutes. Measurements performed before and after sonication indicated that the thermal conductivity was not affected by bath sonication. All samples were stable and no sedimentation occurred during the experiments. The nanotube suspensions were prepared in two steps. First, sodium dodecylbenzene sulfonate, NaDDBS (95% purity, #289957, Sigma-Aldrich, Inc.) was mixed with water at mass fractions ranging from 10 to 200 g/L. The mixtures were sonicated and stirred vigorously until the surfactant was dissolved completely. Then, MWNTs were added to the solution to obtain nanofluids with particle volume concentrations from 0.01% up to 1%.

Each data point was obtained by taking 5 consecutive measurements, with 5 minute intervals in between to allow the sample to re-equilibrate with the water bath (FS60 by Fisher Scientific Inc.). We estimate the standard deviation of the mean conductivity

Table 3.1: NaDDBS and MWNT concentrations

	Surfactant concentration at different surfactant-to-carbon nanotube mass ratio			
CNT volume fraction	5X	10X	20X	100X
0.01%	1.0 g/L	2.0 g/L	4.0 g/L	20.0 g/L
0.02%	2.0 g/L	4.0 g/L	8.0 g/L	40.0 g/L
0.03%	3.0 g/L	6.0 g/L	12.0 g/L	60.0 g/L
0.05%	5.0 g/L	10.0 g/L	20.0 g/L	100.0 g/L
0.08%	8.0 g/L	16.0 g/L	32.0 g/L	160.0 g/L
0.1%	10.0 g/L	20.0 g/L	40.0 g/L	200.0 g/L
0.2%	20.0 g/L	40.0 g/L	80.0 g/L	—
0.5%	50.0 g/L	100.0 g/L	200.0 g/L	—
1.0%	100.0 g/L	200.0 g/L	—	—

to not exceed 0.015 W/mK for micro suspensions and 0.010 W/mK for nanofluids. To ensure that the suspensions were dilute so that particles were unlikely to interact thermally with one another we prepared suspensions of volume fraction only up to 1% for nanofluids and 5% for suspensions containing micron-sized particles. For long dispersed objects, not only particle interaction but percolation is possible if the suspension is concentrated enough. This might provoke significant heat transport augmentation in nanofluids. However, the suspensions used in present study are diluted enough for particles to experience no direct tube-tube interactions. The transition from this "dilute" mode to the regime with different tube-tube interaction behavior, "semi-dilute," occurs at volume fraction defined as following [26]:

$$\phi_0 = 24(\frac{d}{L})^2 = 24\frac{1}{a^2}, \tag{3.2}$$

where d and L are the diameter and length of the nanotube correspondingly. The aspect ratio a is the ratio of the particle length to its diameter in this case. It will be shown later that average diameter of nanotubes used in present study is 22 nm, while the average aspect ration was measured to be 33. The critical volume fraction is about 2.5 % in this case, which is above the maximum volume fraction of 1% we used in our experiments. The critical volume fraction for our dispersions containing micron-sized

SiC whiskers, in which the particle aspect ratio was found to be 9.6, is 26%. Since we capped our experiment at 5% volume fraction, the micro-particle suspensions can be also considered to be "dilute". Thus we conclude, that the concentration of solids content in both nano- and micro-fluids fall well below the critical fraction calculated using Eq. 3.2. This means that particles in suspensions are isolated one from another and can be considered non-interacting mechanically, $i.e.$ are unlikely to form a percolated network. The uncertainty in the solid-content volume fraction is estimated to be 0.001%. This uncertainty comes from measurement of the volume of the suspending fluid and the mass of the suspended phase.

As was mentioned before, another simple "rule of thumb" defines a critical volume fraction at which percolation starts in composite materials, as following [27]

$$\phi_0 = \frac{1}{a}. \tag{3.3}$$

According to Eq. 3.3, CNTs can form a percolated network at volume concentrations above 3%. For SiC whiskers this number is even higher - 10% vol. These are above our particle concentration of 5% for SiC and 1% for MWNTs. Particles at such low concentrations can be also considered to be non-interacting thermally as was shown before using Bruggeman iterative approach. Such simple estimate allows us to conclude, that our suspensions, both nano- and micro-, are not likely percolated and we can use models for predicting thermal conductivity in composites with well-dispersed, thermally isolated particles.

3.2 Error Analysis

Some recent studies explained the enormous increase in thermal conductivity of nanofluids by the possible faultiness of hot-wire method [28]. Nevertheless, recent data by Li *et al.* shows that hot-wire results are in a good agreement with data obtained with steady-state cut-bar for Al_2O_3 aqueous nanofluids at room temperature [29]. Also,

Louge and Chen showed recently that particle migration due to the temperature gradient away from the hot wire toward cold regions, so-called positive thermophoresis, cannot be responsible for the anomalous increase in the thermal conductivity of nanofluids [30]. Thus we conclude, that the hot-wire technique used in the present study is an accurate method for measuring thermal conductivity.

Even though the declared accuracy of the KD-2 is 5%, our calibration data shown in Fig. 3.1 indicates that the error in measuring the mean thermal conductivity of suspension can be small due to very good repeatability of the measurements. We can use student's t-distribution to examine the confidence interval for mean thermal conductivities and estimate the limits of the expected mean values. The standard deviation of the mean measured thermal conductivity is given by

$$\sigma = \sqrt{\frac{1}{N-1}\sum_{i=1}^{4}(k_{\mathrm{i}} - \bar{k})^2}, \tag{3.4}$$

with N=5 since the averaging was done using 5 consecutive data points.

We estimated the 95% confidence interval for the expected mean thermal conductivity using the following formula:

$$\bar{k}_{\mathrm{expected}} = \bar{k} \pm t_{4,95}\frac{\sigma}{\sqrt{N}}, \tag{3.5}$$

where $t_{4,95}$ is a corresponding t-value with four degrees of freedom. The calibration data presented on Fig. 3.1 are the mean thermal conductivities obtained by averaging over 5 measurements and the error bars indicate the 95% confidence interval for the expected mean value. This magnitude of error can adequately describe the thermal-conductivity enhancement in the SiC whiskers suspension, where the increase in conductivity was measured to be as high as 85%. However, the thermal conductivity was increased by only 15% and 8% in SiC spheres and MWNTs suspension correspondingly. Nevertheless, the thermal conductivity measurements in both micro- and nanofluids were also repeatable within very narrow intervals which allows us to conclude that the measured thermal conductivity increases were because of the heat transfer

enhancement in these fluids, not due to the experimental error. The standard deviation of the mean thermal conductivity was calculated using Eq. 3.4 to be below 0.015 W/mK for the thermal conductivity measurements of the SiC suspension and did not exceed 0.010 W/mK for MWNTs dispersions. Thus, although the uncertainty in any one measurement is large compared to the measured increases in thermal conductivity for MWNT and SiC sphere suspensions, the uncertainty in the mean thermal conductivity is nonetheless small due to repeated measurements. We estimated the limits of the 95% confidence interval for the mean thermal conductivities and compared them with measured thermal conductivity enhancements as shown in Table 3.2.

Table 3.2: The confidence interval for expected thermal conductivity enhancements

Suspension	$[k/k_{\mathrm{b}}]_{\mathrm{maximum}}$	95% confidence interval for thermal conductivity enhancements
SiC spheres	15%	±3.1%
SiC whiskers	85%	±1.8%
MWNTs	8%	±0.8%

It can be seen clearly from the Table 3.2, that even though the thermal conductivity enhancements in suspensions containing SiC spheres and MWNTs are only two or three times higher than declared (single-measurement) accuracy of the measuring equipment, the expected mean values fall within narrow confidence intervals. This allows us to conclude that the measured enhancements in thermal conductivity that we will discuss in the following chapters are real and statistically significant.

The last part of this research involves some real-time measurements of thermal conductivity. However, the duration of any single measurement of around 1.5 minutes is much smaller than the timescale of any changes in the suspensions. Again, this allows us to conclude that any changes in measured thermal conductivities are attributable to the heat-transfer augmentation.

Chapter 4

Principal Parameters

In order to compare the experimental data obtained in this study with the theoretical predictions, several parameters must to be known:

1) Thermal conductivities of both dispersed and dispersing media;

2) Kapitza resistance at particle/liquid interface;

3) Size and geometry of particles.

4.1 Thermal Conductivities of Mixing Media

As for thermal conductivity of base fluids, we measured them directly. The thermal conductivity of ethylene glycol was found to be 0.25 W/mK, which is consistent with literature values [25]. The thermal conductivities of the base fluids for dispersing MWNTs varied with surfactant concentration and were measured for each sample separately, as shown in Fig. 4.1.

The thermal conductivities of the suspended particles were obtained from analysis of the existing experimental literature. Yet there is no direct data available for for nano- and micro-particles of SiC. Bulk silicon carbide is a semiconductor that is considered to have a very high thermal conductivity. However, data reported for the thermal conductivity of SiC vary by almost four orders of magnitude, from 0.12 up to 490 W/mK at room temperature, with the actual value depending on the synthesis technique, impurity content and material structure. The thermal conductivity of single crystal SiC has reported to be as high as 490 W/mK [31, 32], but phonon scattering by electrically active impurities such as Al or N can significantly reduce thermal

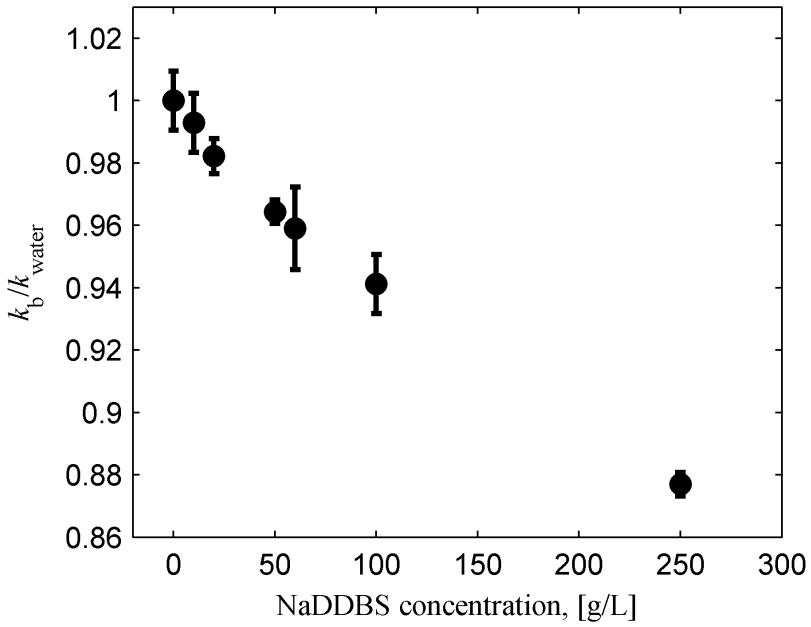

Figure 4.1: Measured thermal conductivities of aqueous bases for dispersing MWNTs at different fractions of surfactant

conductivity. At room temperature, the impurity concentration of 10^{-20} cm^{-3} can reduce the thermal conductivity by the factor of 20 [31]. The thermal conductivity of silicon-carbide polytypes has been measured to be up to 1100 W/mK for different temperatures. However, silicon-carbide thin films, which have amorphous structure, typically have much lower thermal conductivities than that of the bulk material. Measurements [33] showed values of 1.44-1.49 W/mK for 500-nm-thick films fabricated at 20 ^{o}C and 500 ^{o}C correspondingly. An even lower value of thermal conductivity, 0.12 W/mK was reported for optically thin SiC film [34]. The SiC particles used in the present study have crystalline structure, hexagonal for the spherical particles and cubic for whiskers. Therefore, we chose a value of k_p=360 W/mK [31, 35], which is the reported thermal conductivity of a cubic SiC polycrystal at 300 ^{o}C.

As for thermal conductivity of MWNTs, a wide range of conductivities have been reported recently as well. Measurements using a microfabricated suspended device by Kim *et al.* [36] and Small *et al.* [37] found that thermal conductivity exceeded 3000

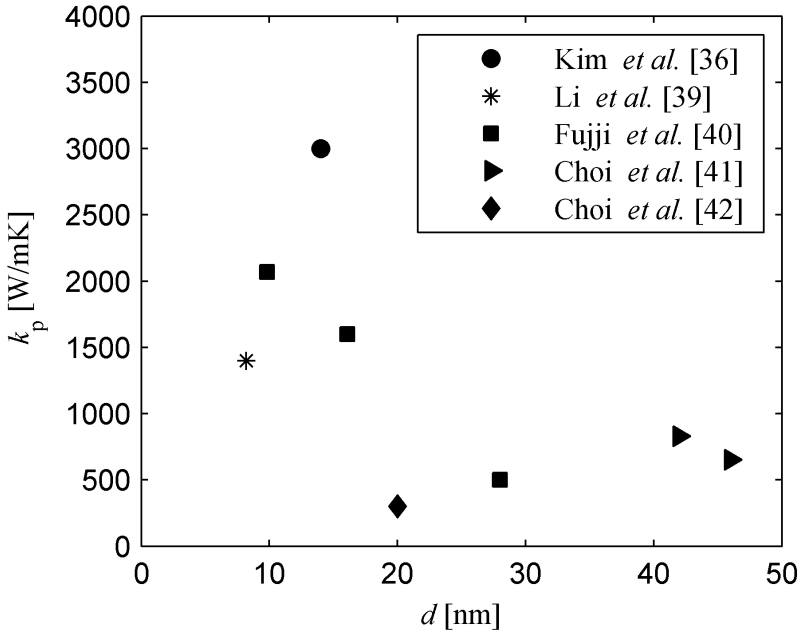

Figure 4.2: Reported thermal conductivities of MWNTs

W/mK for individual MWNT with diameter of 14 nm. At the same time thermal conductivity of MWNTs bundles was found to be well above 1000 W/mK for MWNTs bundles of 80 nm in diameter and around 200 W/mK for 200 nm in diameter bundles. It should be noted that the length of the nanotube, suspended on the device bridge, was equal to 2.5 microns. This result should be even higher if thermal contact resistance (TCR) at the nanotube- measuring device junction is taken into account [38]. To avoid effect caused by TCR Li *et al.* [39] recently introduced non-contact Raman-spectra-shift method. The thermal conductivity of an extremely long MWNT with length L=60 microns and diameter d=8.3 nm was found to be 1440-2500 W/mK. In general, the thermal conductivity of CNTs decreases with the diameter and the number of carbon layers. Fujii *et al.* [40] showed that k_p of MWNTs dropped from 2069 W/mK to around 500 W/mK for diameter ranging from 9.8 to 24 nm. The thermal conductivity of nanotubes also increases with nanotube length but saturates at some length. Choi *et al.* measured the thermal conductivity of MWNTs with 3-ω method. They found thermal conductivity to be equal 630 W/mK for nanotube with d=43 nm

and length of 1 micron [41]. Thermal conductivity of slightly thinner and longer nanotubes turned out to be higher, 830 W/mK, as expected. Later experiment by the same group showed even lower value for thermal conductivity of MWNTs with diameter of 20 nm [42]. They measured the thermal conductivity to be equal 300 W/mK. In this study Choi *et al.* utilized the four-point-probe third-harmonic method which eliminates the TCR effect as compared to the regular 3-ω technique. Surprisingly, thermal conductivity turned out to much lower than measured with regular 3-ω method even though the diameter of MWNTs was half of that used in the previous experiment, even though the effect of the contact resistance is supposedly eliminated. A number of experimental studies have also reported slightly lower values for thermal conductivity of MWNTs. For example, Shioya *et al.* found k_{p} = 950 W/mK for 10-nm in diameter tubes measuring thermal conductivity of MWNTs pillars [43]. Yang *et al.* measured thermal conductivity of MWNTs to be as low as 200 W/mK, but no information was provided about tube diameter [44]. However, both Shioya *et al.*'s and Yang *et al.*'s results can be referred as in-direct methods, *i.e.* the resulting thermal conductivities of individual tubes were calculated after measuring thermal properties of MWNTs pillars and films correspondingly. These methods might result in less accurate data than those obtained with direct methods of measuring the thermal conductivity of individual CNTs using microfabricated devices [42], [36], [37], [40]. Therefore, multi-walled nanotubes thermal conductivity differs by the order of magnitude from the one experiment to another. We summarize the above data in Fig. 4.2 for conductivities obtained from a single nanotube's conductivity measurements. Although reported thermal conductivities differ, it is apparent in general that the conductivity of MWNTs depends on nanotube diameter (decreasing with increasing number of carbon layers) and length (nevertheless saturating at some length). Based on the data presented in Fig. 4.2, we conclude that k_{p} = 1000 W/mK is the reasonable estimate of the thermal conductivity of our MWNTs, which have a volume-weighted average diameter of 21.6 nm. Higher thermal conductivities were only reported for single-walled nanotubes

and multi-walled nanotubes with diameter less than 10-15 microns, while lower thermal conductivities were typically only reported for thick nanotubes (with the exception of one of Choi *et al.*'s results [42] among data obtained with direct methods). For the moderate aspect-ratio particles of the present study, variations in the value of k_{p} about the estimated value of 1000 W/mK would have a minimal effect on the thermal conductivity of the suspension, as discussed in the next chapter. It should be noted that the data in Fig. 4.2 represents the thermal conductivity in the direction along the axis of the carbon nanotube. The measured thermal conductivity in radial direction is much less and is comparable with the thermal conductivity of graphite [44], [45]. We use a value of 5.6 W/mK for radial thermal conductivity in our calculations [45].

4.2 Interfacial Resistance

In the case of energy transport, continuum theory assumes continuity in both temperature and energy flux across the interface. This assumption is valid at macroscopic scale, but breaks down as the characteristic length decreases to nanometers. The interfacial thermal resistance becomes more and more important as the size of dispersed particles decreases since the total surface area of particle/liquid interfaces is increasing. A more transparent explanation of interfacial phenomena involves Kapitza length, which is the thickness of a liquid or solid layer equivalent to the interface from the thermal point of view, *i.e.* Kapitza length is defined as

$$l_{\mathrm{K}} = k_i R_{\mathrm{K}}, \tag{4.1}$$

where k_i is either k_{p} or k_{b}.

When Kapitza length is large compared to the problem characteristic dimension, such as particle size, the contact resistance plays an important role in thermal transport. In the case of nanofluids, especially containing nanotubes, thermal conductivity of dispersed phase is extremely high, which means some measurable effects due to interface heat transport can be expected. More important, Kapitza length becomes more

comparable to the size of the particle/tube as this size decreases. For most liquid/solid interfaces the Kapitza resistance is typically of the order 10^{-8} $\mathrm{m^2K/W}$. The thermal contact resistance of the interface was found to be in a range $4.5 - 14.7 \times 10^{-8}$ $\mathrm{m^2K/W}$ by molecular dynamic (MD) simulations on single-walled nanotubes (SWNTs) in octane [46]. Simulations were performed on nanotubes constructed from 100 to 720 carbon atoms, corresponding to the tube length from 122 to 720 nm. Two different approaches, constant heat rate and relaxation simulations, used in MD simulations reproduced each other. The model used in calculations is representative for liquids with slightly or non-polar molecules, polymers. MD simulations of thermal contact resistance are in a good agreement with experimental data obtained by Huxtable *et al.* [47], who found $R_{\mathrm{K}} = 8.3 \times 10^{-8}$ $\mathrm{m^2K/W}$ for CNTs dispersed in water with the aid of sodium dodecyl sulphate (SDS). However, there is currently no data on the interfacial resistance of NaDDBS-stabilized carbon nanotubes in aqueous suspension. As for the interfacial resistance in other nano-scale systems, R_{K} values above 10^{-8} $\mathrm{m^2K/W}$ are usually referred only to weakly bonded (such as hydrophobic) interfaces [34]. For strongly bonded interfaces (for example, AuPd nanoparticles in water) reported resistances are around 10^{-8} $\mathrm{m^2K/W}$ and even lower [48], [49]. Molecular dynamics simulations for the wetting systems have reported on small magnitude of interfacial resistance that corresponds to the Kapitza length of only ≈ 1 nm[50]. This allows us to expect lower interfacial resistance values for stabilized suspensions where surfactant molecules are strongly adsorbed on nanotube surface. For a base fluid of thermal conductivity $k_{\mathrm{b}} = 0.56$ W/mK and Kapitza resistance of 8.3×10^{-8} $\mathrm{m^2K/W}$, a typical Kapitza length would be about 40 nm, which is somewhat comparable to the nanotube diameter. For the micro-suspension used in a present study, where k_{b}=0.28 W/mK, a Kapitza length of 20 nm is smaller than either a diameter of SiC whiskers or size of SiC sphere. This is why, interfacial resistance, essential in the case of CNTs suspension, is negligible for micro-fluids. In all our calculations for SiC whiskers and spheres we neglect this effect.

4.3 Particle Morphology

In order to carry out a full comparison of experimental data with theory, we need to know the morphology of the particles suspended in fluid. The size of the dispersed phase does not affect the thermal conductivity according to Maxwell or Fricke [15], [19]. However, particle size is essential parameter for determining if the interfacial resistance on liquid/solid interface has a significant impact on thermal conductivity of nanofluid [10], [13]. For both nano- and micro-fluids, however, the aspect ratio of dispensed particle is predicted by theory to have a great effect on thermal conductivity.

The actual aspect-ratios of the SiC whiskers in suspension were determined from optical micrographs, as seen in Fig. 4.3. A very thin layer of a diluted EG suspension was deposited between two microscope slides. Images were taken at magnification of x10 and x20. Particle-size analysis of N=250 randomly chosen SiC whiskers showed a wide distribution of particle aspect ratios, with average volume-weighted aspect ratio of 9.6. For comparison, the simple average aspect ratio is equal 5.71. The measured aspect-ratio distribution for SiC - EG suspension is shown in Fig. 4.6. The average size of these particles (Fig. 4.4), which are the particles of angular morphology actually, was measured to be 32 microns. Sample size distribution for spherical particles is shown in Fig. 4.5.

To vary the aspect ratio of the SiC whiskers, the suspension at volume fraction of $\phi = 0.025$ was further processed in a ball mill. The ball mill, consisting of a rotating horizontal cylinder partially filled with a milling medium (in this case, ceramic balls with diameter of 7 mm), reduced the whiskers' aspect ratio by grinding. The SiC whisker suspensions were processed for 4, 12 and 28 hours, and the average volume-weighted aspect ratio of the whiskers was calculated after every step from images taken with an optical microscope (Fig. 4.3).

Figure 4.6 shows the distribution functions of whisker aspect ratios for the sample after 0, 4, 12 and 28 hours of milling. Milling causes a decrease in the amount of long particles, since whiskers break from the contact with ceramic balls. It can be clearly seen that, after 48 hours of grinding, the fraction of very short particles is almost twice

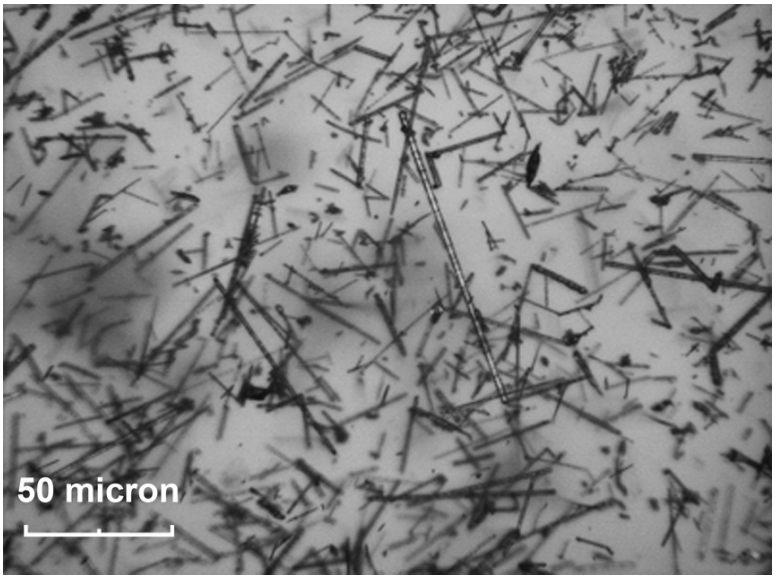

(a) Whiskers, before milling

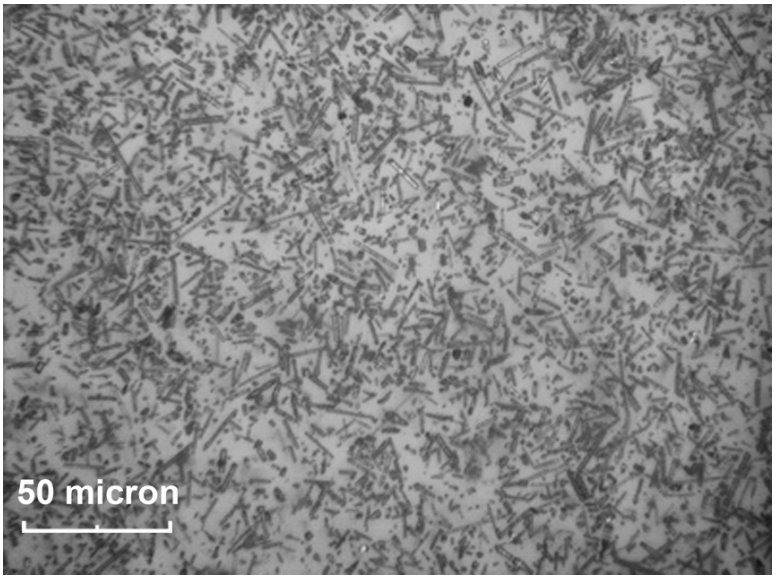

(b) Whiskers, after 28 hrs of milling

Figure 4.3: Optical micrographs of SiC - EG suspensions

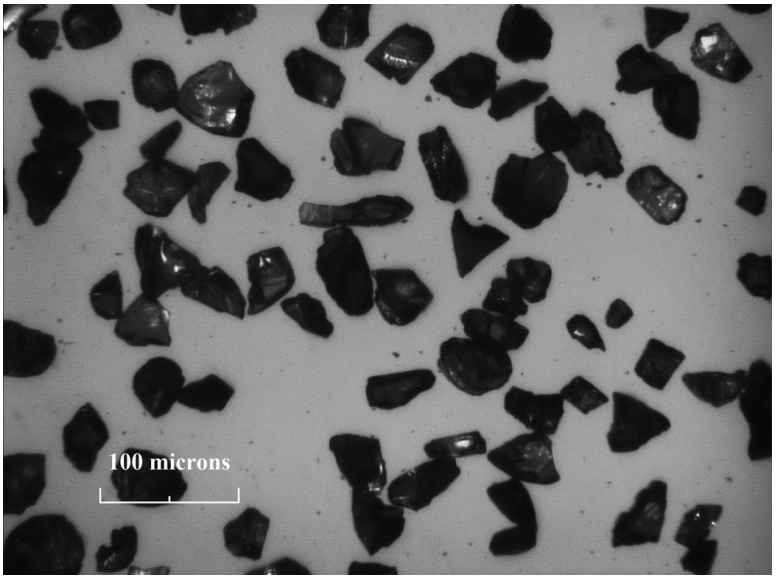

(a) x10

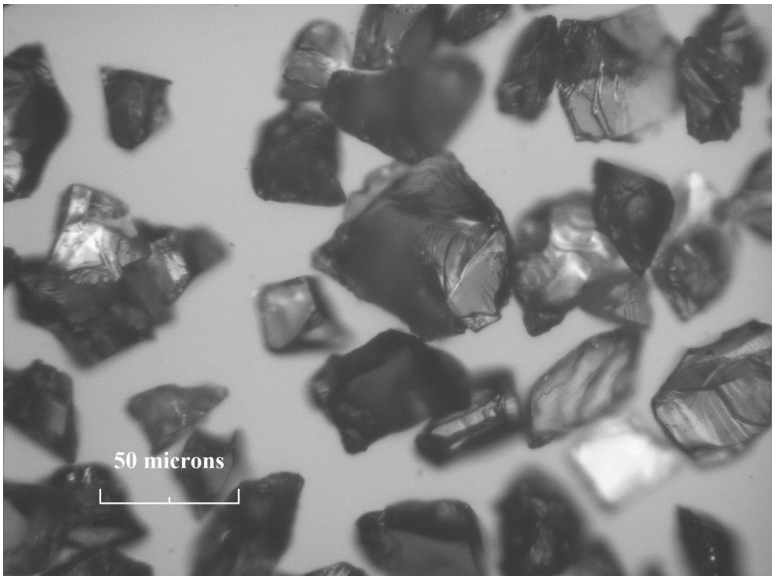

(b) x20

Figure 4.4: Optical micrographs of suspensions containing SiC spheres at different magnifications

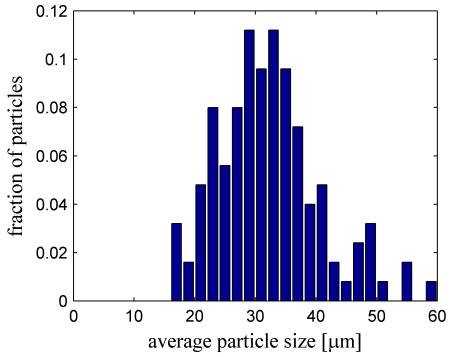

Figure 4.5: Size distribution for SiC spherical particles

Table 4.1: Measured aspect ratio of SiC whiskers

Milling Time, hrs	Average aspect ratio	Standard Deviation	Volume-averaged aspect ratio	Volume-weighted standard deviation
0	5.71	4.75	9.65	7.41
4	4.67	4.08	8.23	5.95
12	3.65	3.01	6.12	5.15
28	2.93	2.37	4.85	3.58

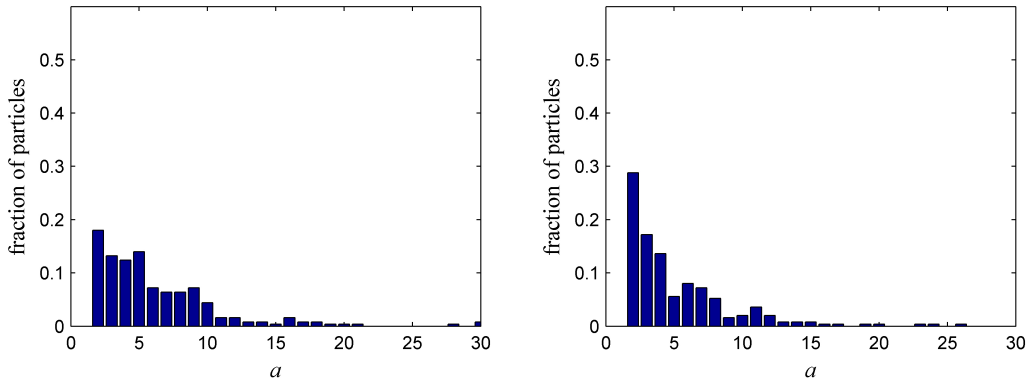

(a) Whiskers, before milling

(b) Whiskers, after 4 hrs of milling

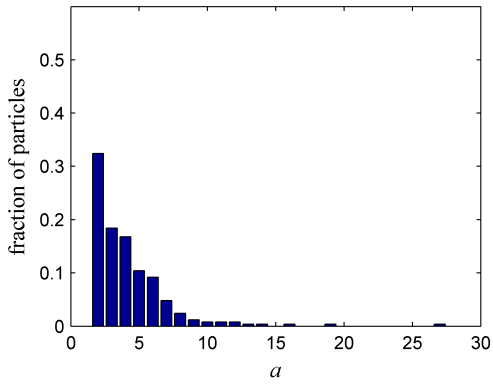

(c) Whiskers, after 12 hrs of milling

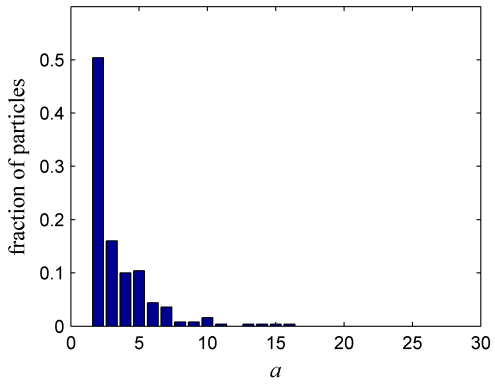

(d) Whiskers, after 28 hrs of milling

Figure 4.6: Measured aspect ratios of SiC whiskers

higher than before. At the same time the fraction of particles with aspect ratio more than 10 decreased significantly. Values of the volume-weighted average aspect ratio, and the corresponding grinding times, are calculated from Eq. 2.19 and listed in Table 4.1. The average aspect ratio was found to decrease gradually from 9.6 down to 4.8 with milling (Fig. 4.6). It can be seen from Fig. 4.6 that short whiskers with aspect ratio less than 10 make up the majority of all particles. The table shows also calculated simple average aspect ratios, which are significantly smaller than the volume-averaged aspect ratios. It is explained in detail in Section 2 why the volume-weighted average aspect ratio is the correct measure to use in calculations rather than the simple average aspect ratio.

Multiwalled nanotubes used in the second part of this study are considered to be short with a nominal length of 0.5-2 microns. A nominal outer diameter of 30-50 nm gives aspect ratios ranging from 10 to around 70. Such short nanotubes are believed to be better dispersible then those of higher aspect ratio and are likely to be easier to characterize. Again, the actual size and aspect ratio of CNTs have to be known exactly. We determined the actual CNT diameter and length from images obtained with Transmission Electron Microscope (TEM). In order to carry such analysis, one part of a nanofluid was diluted with 100 parts of ethanol. The resulting suspension contains around 10^{10} tubes per mL of ethanol which is suitable for proper TEM analysis but remains stable over a long period of time due to very low particle number density. Micrographs (Fig. 4.7) acquired with a JEM 1230 microscope (Japan Electron Optics Ltd.) represent images of a sample obtained from suspension containing originally 0.1% CNTs by volume. Five TEM images of this sample were analyzed and the diameter and length of a total of 216 CNTs were measured. It can be clearly seen from Fig. 4.7 that the majority of tubes are slightly bent or curved; therefore both end-to-end and contour lengths together with diameter were measured for every particle. The obtained diameter of the individual nanotube ranged from 12 up to 35 nm, while the length was as high as 1.4 microns. Using the aspect ratio distribution (Fig. 4.8(a)) we calculated volume-weighted average aspect ratio to be 32.94.

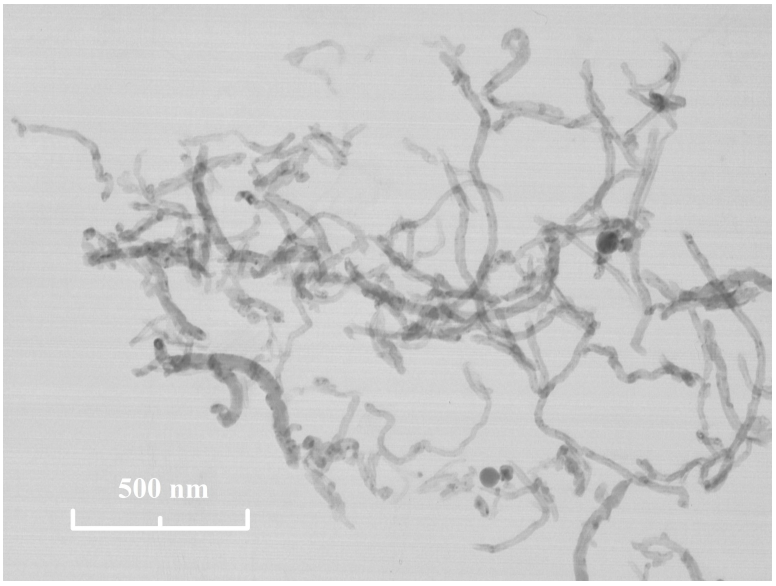

(a)

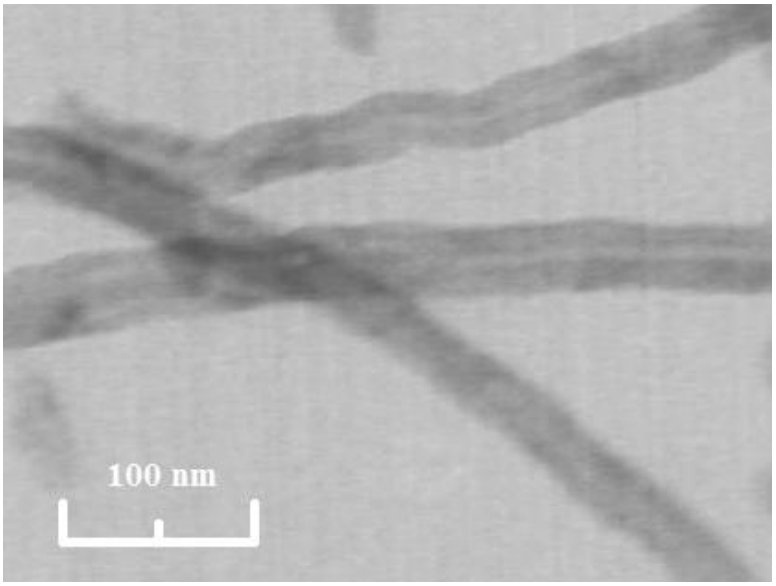

(b)

Figure 4.7: TEM micrographs of MWNTs deposited from suspensions

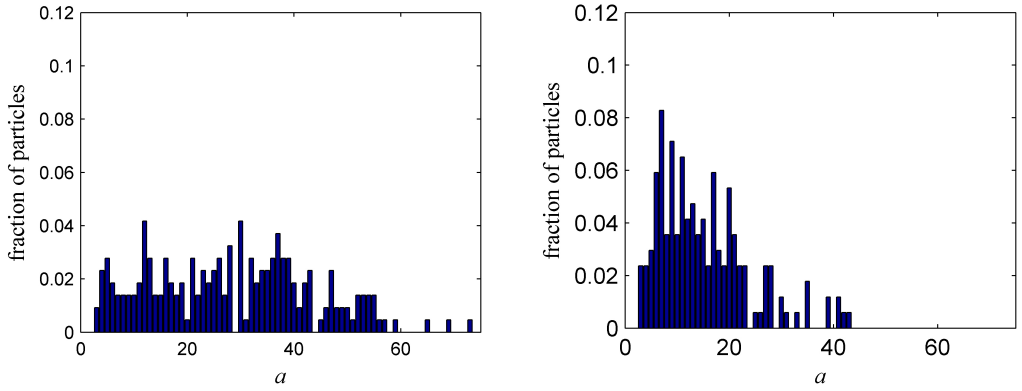

(a) MWNTs, before sonication

(b) MWNTs, after 5 min of sonication

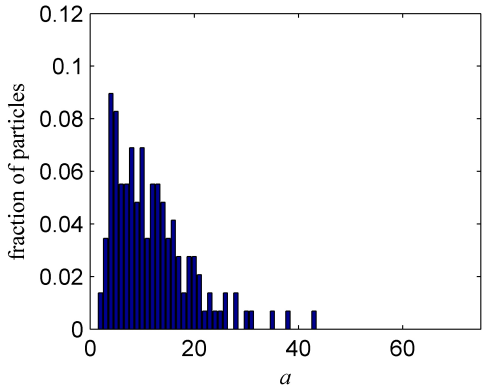

(c) MWNTs, after 10 min of sonication

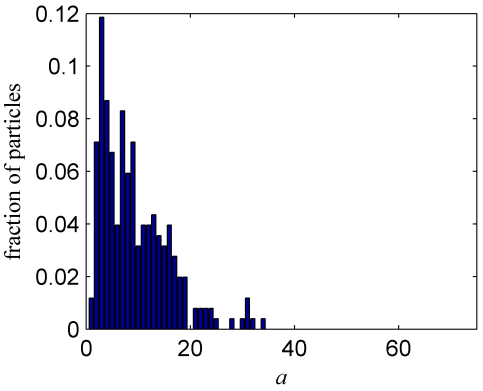

(d) MWNTs, after 15 min of sonication

Figure 4.8: Measured aspect ratios of MWNTs

Table 4.2: Measured aspect ratio of MWNTs

Tip-sonication time, min	Average aspect ratio	Standard Deviation	Volume-averaged aspect ratio	Volume-weighted standard deviation
0	28.04	15.63	32.94	13.10
5	14.61	8.80	20.34	9.94
10	11.42	7.53	15.02	8.42
15	8.92	6.57	14.47	8.15

To investigate the aspect ratio effect on thermal conductivity of nanofluids, we attempted to reduce the nanotube length by sonication. Intensive ultrasonication with tip-sonicator not only disperses nanotubes agglomerates, but also is efficient in breaking the tubes. Milder bath-sonication is reported to have little effect on nanotube structure and is used widely for dispersing nanotubes [51], while more powerful tip-sonication is a typical method to shorten CNTs [24], [52]. Experiments by Yang and Han show a reduction in nanotube aspect ratio from 300 down to 49 after only 5 minutes of tip-sonication of an oil-based MWNT suspension [24]. Further shortening to a=30 was obtained after an additional 25 minutes of ultra-sonication. In this study, we used tip-sonication to reduce the aspect ratio of the MWNTs in aqueous dispersion and to further investigate the thermal conductivity of a MWNT suspension with fixed nanotube volume fraction, but varying particle shape. The sonication time in our experiment varied from 5 to 15 minutes in high-power sonication machine.

We compared suspensions containing 0.1% MWNTs by volume and 10X fraction of surfactant by weight, because this sample showed significant stability against aggregation and sedimentation. Unlike the bath sonication we used for initially dispersing the nanotubes, the tip-sonication (W-385 Ultrasonic Processor by Heat Systems Ultrasonic, Inc.) was very intense and accompanied by extensive cavitation and heating. All samples were allowed to cool every 5 minutes to minimize effects due to elevated temperature. For every sample, the nanotube diameter, contour length L_{C}, and end-to-end length L_{EE}, which was used for calculating the aspect ratio, of at least 145 nanotubes were measured from several TEM micrographs (Table 4.2). Aspect ratio

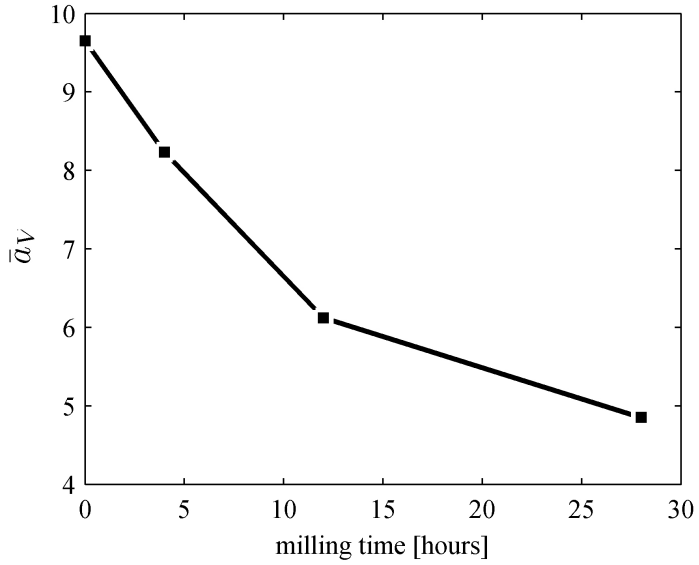

(a) Aspect ratio of SiC whiskers *vs.* time of grinding in a ball mill

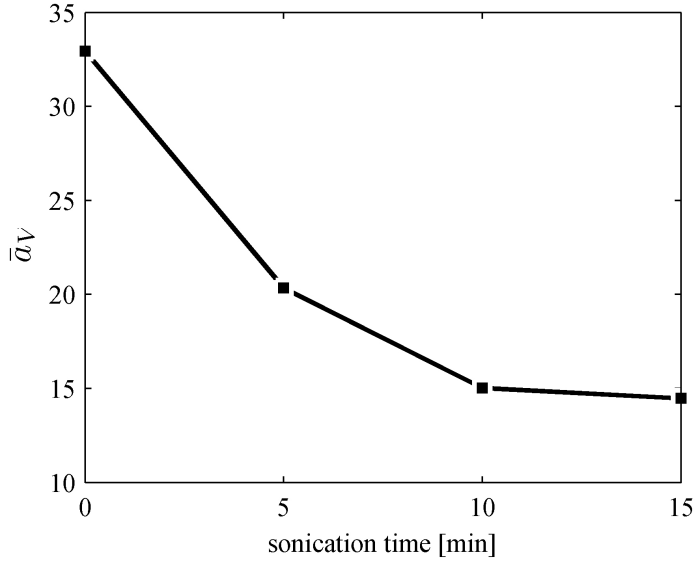

(b) Aspect ratio of MWNTs *vs.* sonication time in a tip-sonicator

Figure 4.9: Measured aspect ratios of whiskers and nanotubes

distributions are shown in Fig. 4.8. The volume-averaged aspect ratio was then calculated from the measured aspect-ratio distribution for each sample. As seen in Fig. 4.8, the initially broad aspect-ratio distribution narrowed and shifted toward shorter particles after sonication. After 5 minutes of sonication, the volume-averaged aspect ratio decreased to 20 and was ultimately reduced by a factor of 2 after a total of 15 minutes of sonication (Table 4.2).

Chapter 5

Thermal Conductivity Measurements

As the first step of this study we investigated thermal transfer enhancement in microfluids containing SiC particles of different shapes. In this case, when the size of dispersed particles is of the order of few microns, we can neglect Kapitza resistance on the particle/liquid interface. Thus, we reduce the number of principal parameters affecting the heat transport in such fluids. The measured thermal conductivities of suspensions of spherical and cylindrical SiC particles dispersed in EG at volume fraction up to 5% are presented in Fig. 5.1. It can be clearly seen that suspensions containing cylindrical particles show significantly higher increase in thermal conductivity than suspensions with dispersed spherical particles. For the particle loading of 5% by volume, a thermal-conductivity enhancement of 85% was observed for suspensions containing dispersed whiskers, while the enhancement was only 15% for spheres. Over this low volume-fraction range, the thermal conductivity increase for both types of particles is nearly linear with volume fraction of solids. It is clearly seen in Fig. 5.1 that the Maxwell model for the thermal conductivity enhancement of spheres with k_{p} = 360 W/mK is in a good agreement with our experimental data. It was shown before, that this is the reasonable choice of thermal conductivity for both spherical and cylindrical SiC particles. The Maxwell model, Eq. 2.9, is insensitive to the thermal conductivity of the dispersed phase when the ratio, $\delta = \frac{k_{\mathrm{p}}}{k_{\mathrm{b}}}$, of thermal conductivities of the dispersed and dispersing materials, is greater than ≈ 100, as was shown before. Thus any possible error in thermal conductivity of SiC has minimal effect on the calculated conductivity of the suspensions containing spherical particles. The effective medium theory, Eq. 2.27 is much more sensitive with respect to the thermal conductivity ratio, k_{b}, but the results presented in Fig. 5.1 show a good agreement

of SiC-whisker experimental data with the EMT calculations. For comparison, suspension thermal conductivities calculated using k_{p} = 100 W/mK and k_{p} = 500 W/mK are also plotted in Fig. 5.1. These limiting cases correspond to the small-grain and perfect, single-crystal SiC [31, 53]. It can be seen that the EMT theoretical predictions fit the data well for any reasonable choice of thermal conductivities for the SiC whiskers. As previously discussed, the aspect ratio is taken as a volume-weighted average of a_V = 9.6 for calculations. Thus, we conclude that particle shape has a great effect on thermal conductivity of suspensions. Also, EMT predicts experimental data adequately for micro-fluids, when interfacial resistance is not taken into account.

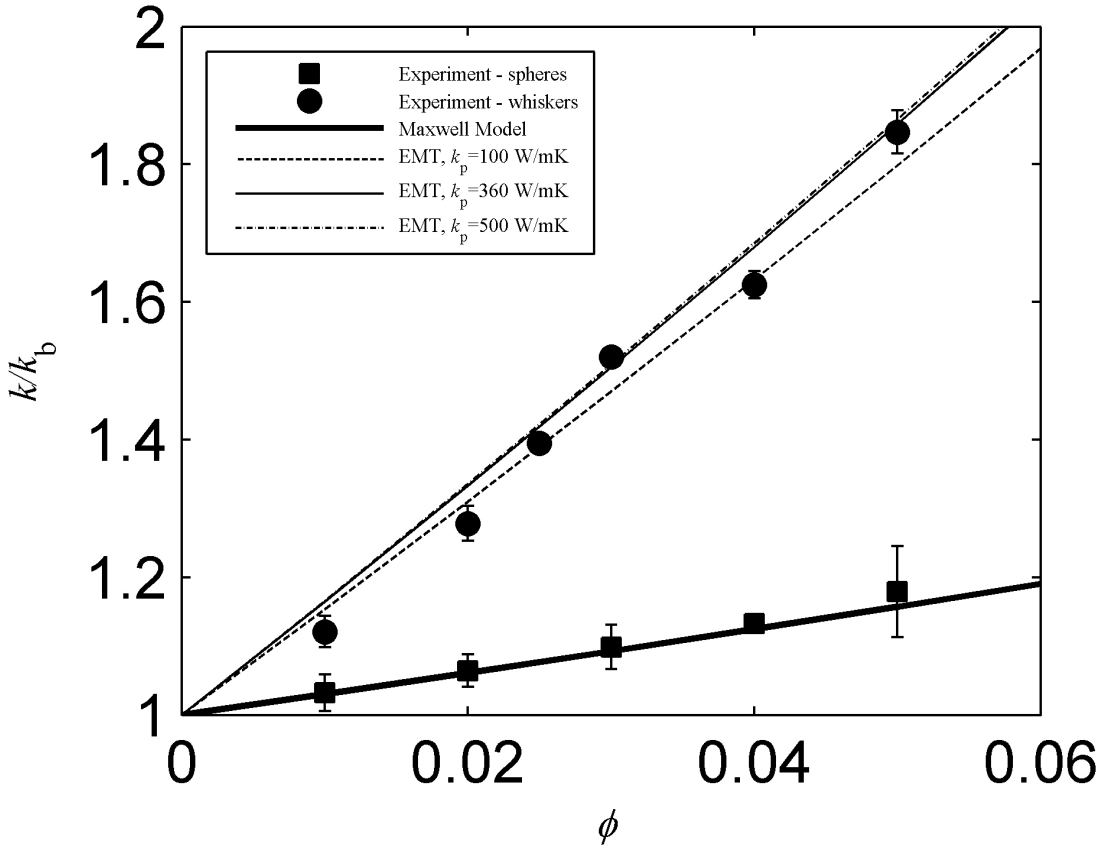

Figure 5.1: Relative thermal conductivity enhancement in the suspensions containing silicon carbide spherical particles (solid squares) and whiskers (solid circles) compared to the data calculated with the aid of Maxwell and EMT for different thermal conductivity of whiskers k_{p}.

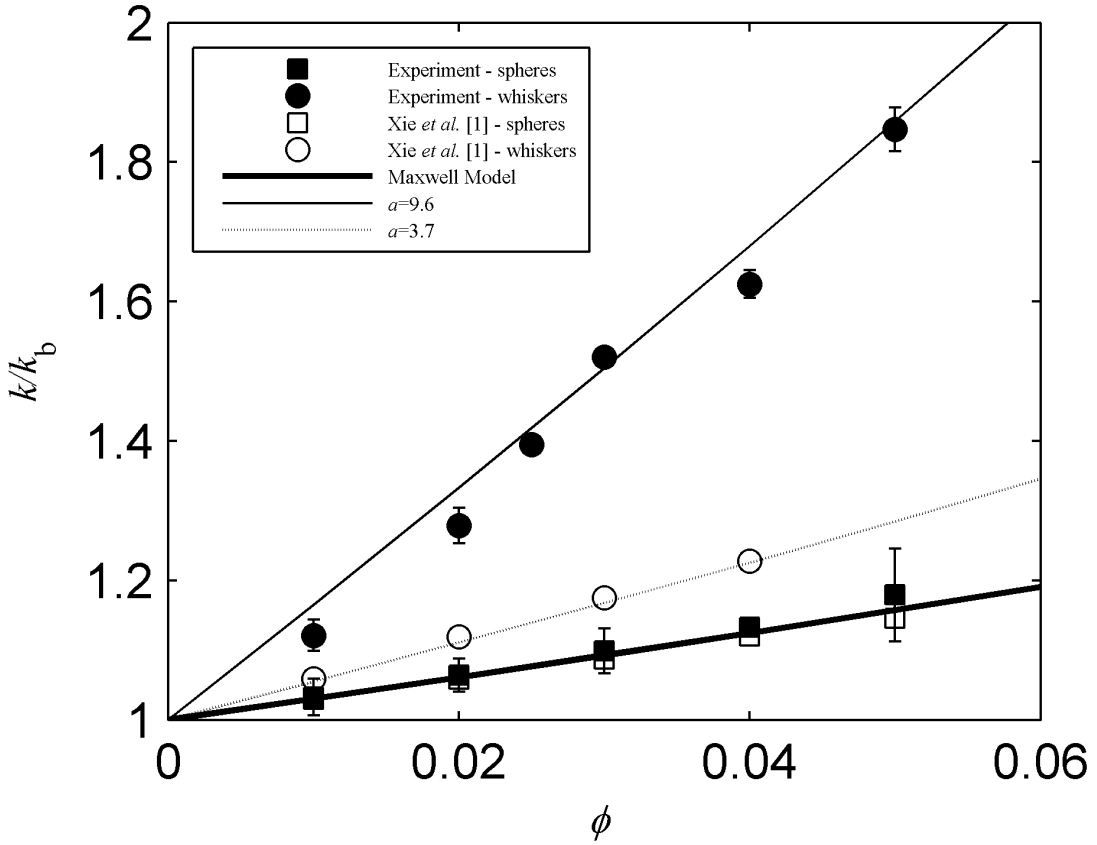

Figure 5.2: Relative thermal conductivity enhancement in the EG-based suspensions containing silicon carbide spherical particles (solid squares) and whiskers (solid circles) compared to the data calculated with the aid of Maxwell and EMT. Data by Xie *et al.* [1] for spheres and cylinders are shown with hollow squares and circles correspondingly. EMT prediction for a=3.7 is shown with dotted line for comparison with Xie *et al.*'s data on cylinders.

For comparison, the experimental data of Xie *et. al.* [1] for suspensions of spherical and cylindrical SiC particles are also shown in Fig. 5.2. For spherical particles, their data and ours match well. For the cylindrical particles, Xie *et al.* do not provide precise information about the exact particle size and shape. Thus, the differences seen in Fig. 5.2 between their data on cylindrical particles and ours most probably arise from the use of particles of different aspect ratios. Nonetheless, their measurements also show an increase in thermal conductivity above the Maxwell prediction when anisotropic particles are used. The thermal conductivities reported by Xie *et. al.* can be fit well by the EMT model if the suspension is assumed to contain SiC whiskers of aspect ratio 3.7, as seen in Fig. 5.2. Despite the difference in the results for cylindrical particles, which might be attributed to the disparity in the aspect ratios, both Xie *et al.*'s data and the results obtained in this study reveal a significant difference in conductivity measured for fluids containing particles of different shape.

Next, we attempt to include the effect of interfacial resistance on particle/liquid interface into consideration. This resistance starts to play an important role as the particle size decreases. So, as the next step of this work, we investigated the thermal conductivity of sodium dodecylbenzene sulfonate - stabilized MWNT-based nanofluids. The diameter of the dispersed particles goes from 1.5 microns for SiC whiskers down by two orders of magnitude for MWNTs. In this case, the Kapitza resistance must be included in calculations in order to compare theoretical predictions and experimental data. For nanotubes, we capped our experiments at 0.01 % to avoid nanotubes percolation. Nanotubes themselves are hydrophobic, aggregate easily and cannot be dispersed into many fluids, including water. Along with many different surface modification techniques, surfactants, or dispersants are widely used to mix nanotubes with water. In the first place, NaDDBS was chosen as surfactant because of its reported effectiveness in dispersing nanotubes in water, as will be discussed in the next section. Our suspensions were prepared with different surfactant-to-nanotube mass ratios as shown in Table 3.1. The mass fraction of surfactant in our suspensions ranged from one up to 200 grams per liter of water. We used surfactant-to-nanotube mass ratios from 5, 10, 20 and 100. The measured thermal conductivities of aqueous suspensions

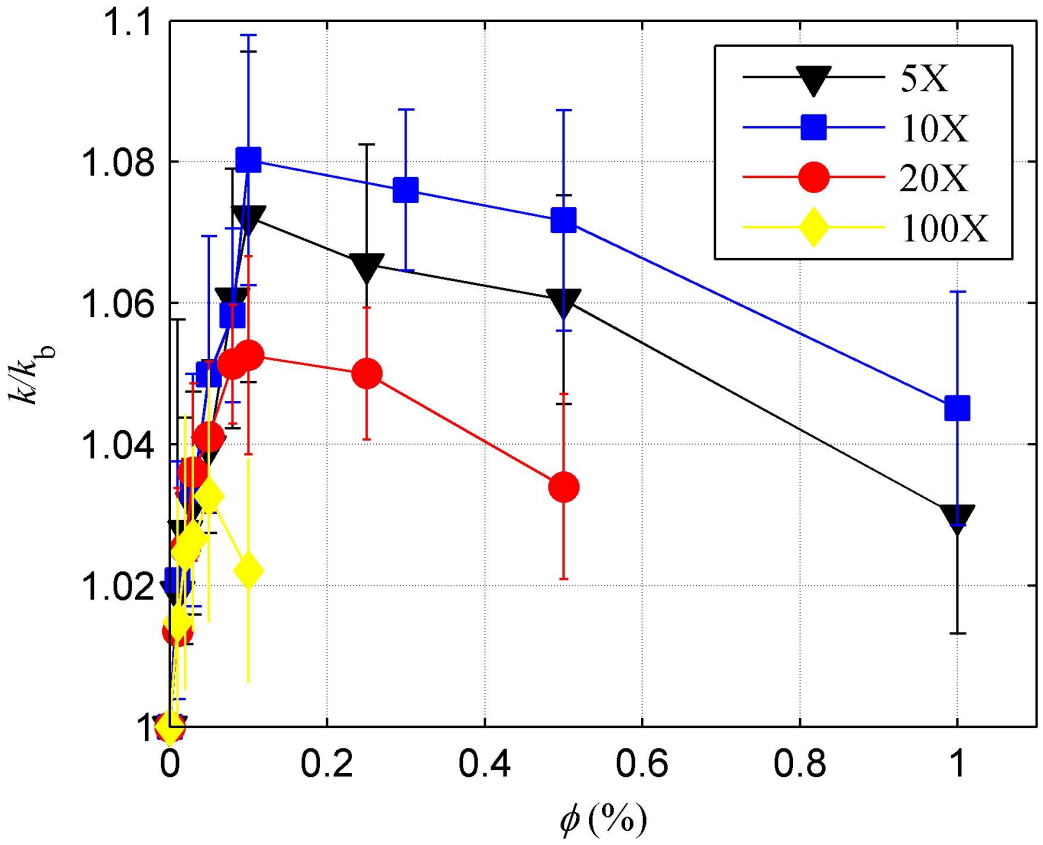

Figure 5.3: Relative thermal conductivity enhancement in the aqueous suspensions containing MWNTs at different surfactant-to-nanotube mass ratios.

containing from 0.01% up to 1% nanotubes by volume are presented in Fig. 5.3. It can be seen that thermal conductivity increases almost linearly for samples containing less than $\sim$ 20g/L of NaDDBS. This regime corresponds to a stable-against-sedimentation nanofluid, as will be discussed in the Chapter 7. In order to compare our experimental data with theoretical predictions, we cap data in Fig. 5.3 by the surfactant concentration 20-50 g/L, because EMT describes the heat transfer mechanism in well-dispersed stable medium.

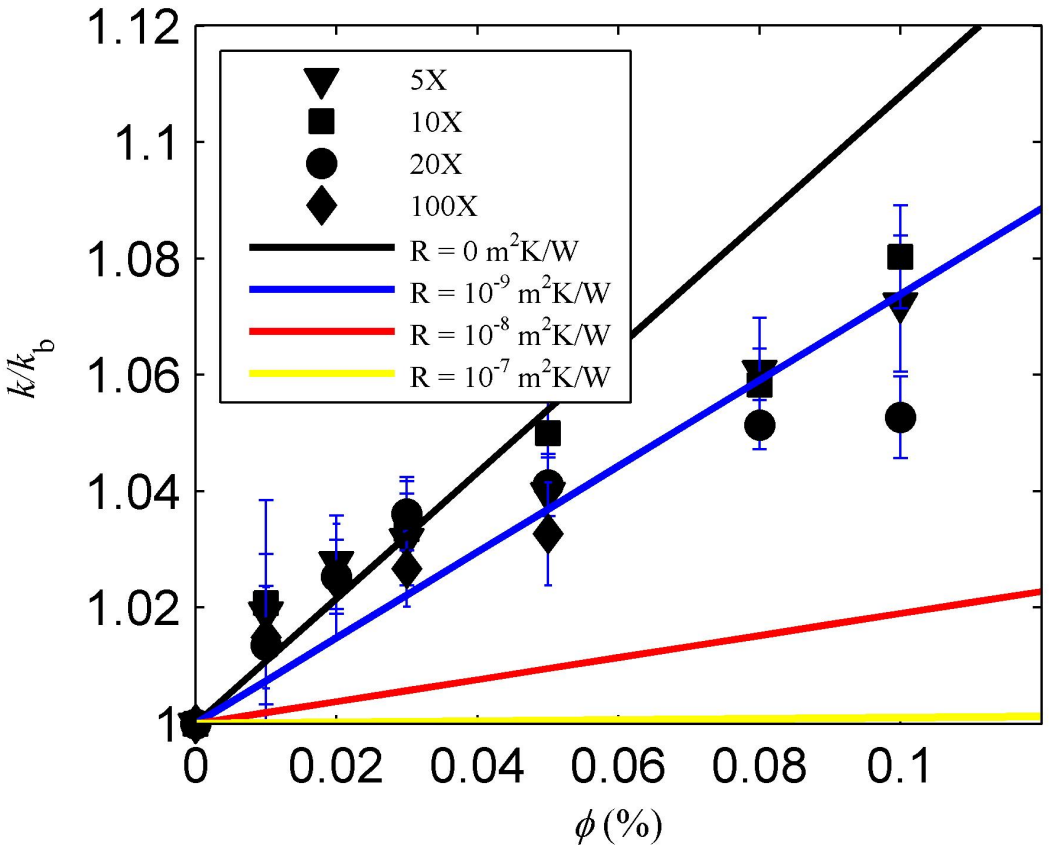

Figure 5.4: Relative thermal conductivity enhancement in the aqueous suspensions containing MWNTs compared with EMT predictions at different magnitudes of interfacial resistance R_{K}

We attempted to compare our experimental data with EMT predictions in Fig. 5.4. For the case of nanofluids, which diameter is of the order of tens nanometers, we cannot neglect the Kapitza resistance on the nanotube/liquid interface as we did for

micron-sized whiskers. Figure 5.4 shows measured thermal conductivities of nanofluids compared with theoretical calculations. It can be seen that measured thermal conductivities are higher than predicted by EMT if Kapitza resistance is within previously reported range [46]- [47] of around $10^{-8} - 10^{-7}$ $\mathrm{m^2W/K}$. Experimental data fit theoretical predictions for interfacial resistance of around 10^{-9} $\mathrm{m^2K/W}$. Even though we do not have data on interfacial resistance for CNTs suspended in water with the aid of NaDDBS, such a difference in R_{K} probably cannot be attributed to the choice of the surfactant only. As was mentioned above, Huxtable *et. al.* report $R_{\mathrm{K}} = 8.3 \times 10^{-8}$ $\mathrm{m^2K/W}$ for CNT suspended in SDS micelle [47], so we expect R_{K} for NaDDBS to be somewhat close to this number. From the other hand, such high magnitude of interfacial resistance can provoke the drop in thermal conductivity of composite material compared to the base medium in some cases. This is true for suspensions of spherical particles with radius less than critical radius R_{K} as followed from Eq. 2.25:

$$R_{cr} = k_{\mathrm{p}} R_{\mathrm{K}} / (\frac{1 - 4\phi}{2\delta(\phi - 1)} - 1) \tag{5.1}$$

However, no experimental study reports on such a decrease in thermal conductivity even for suspensions containing very small particles. This suggests that the true Kapitza resistance is lower than 10^{-8} $\mathrm{m^2K/W}$ previously reported.

Also, there are some additional factors affecting the heat transfer mechanism at nanoscale. One of the possible explanations is that the difference can be attributed to the fact that the model is derived for rigid dispersed particles. MWNTs were believed to behave like rigid rods together with SWNTs because of their exceptionally high Young's modulus. The main parameter characterizing the degree of flexibility for long objects is their persistence length (L_{P}). Only particles shorter than their persistence length can be considered rigid. Some real time visualization experiment [54] showed that L_{P} ranged from 32 up to 171 microns for SWNTs and it was expected to be even higher for MWNTs [55]. However recent experiments showed much lower [56] L_{P} for MWNTs than expected. Lee and Yun measured the persistence length to be only 271 nm for 21 nm diameter MWNTs with volume-weighted contour length of 1.3 microns

[56]. Theoretical calculations by Arroyo *et al.* [57] have found the persistence length $\sim$ 500 nm for MWNTs. We estimate the length of MWNTs utilizing the technique widely used in polymer science. Persistence length of long polymers deposited and equilibrated on a 2-D surface is given by [58]:

$$< L_{\mathrm{EE}}^2 >= 4L_{\mathrm{P}}L_{\mathrm{C}}[1 - \frac{2L_{\mathrm{P}}}{L_{\mathrm{C}}}(1 - \exp^{-\frac{1}{2L_{\mathrm{P}}}})] \tag{5.2}$$

where L_{C} and L_{EE} are contour and end-to-end lengths of nanotubes deposited on a surface. From images of our MWNTs dried onto the TEM grid, we calculated the persistence length for our MWNT samples to be L_{P} = 397 nm, which is considerably shorter than the volume-weighted average length of 771 nm. Since the majority of tubes in our suspensions are longer than L_{P}, the rigid-rods assumption breaks and the nanotubes can experience significant bending due to the thermal fluctuations. This thermally-driven bending motion may enhance heat transfer in this suspension. It should be noted that this motion is not purely Brownian rotation or translation, and is distinct from the Brownian motion effect that has been previously considered as a possible contributor to the thermal conductivity enhancement in nanofluids [12], [59]-[60].

Nonetheless, we have experimentally validated the EMT prediction that the thermal conductivity of a fluid is significantly enhanced by the addition of large aspect-ratio nanotubes. Reasonable agreement is found between the measured and EMT-predicted thermal conductivities, and no anomalous increase in thermal conductivity outside any possible theoretical predictions was detected.

Chapter 6

Aspect Ratio Effect on Thermal Conductivity

As it was discussed in Chapter 4, the aspect ratio of dispersed elongated particles is one of the most important parameters affecting conductive thermal transport in composite materials, including liquid suspensions. The thermal conductivity enhancement of suspensions containing long cylinders can be orders of magnitude higher than of those composed of spheres at the same volume concentration. This is why it is extremely important to determine the real shape and size of the filler particles. Moreover, it is essential to know the distribution of the parameters rather than simple average or mean values, in order to determine the volume-weighted aspect ratio. We obtain the aspect-ratio distribution of SiC whiskers and MWNTs from optical and TEM micrographs, respectively. In the previous chapter we assumed a_V = 9.6 for SiC cylinders and a_V = 32.94 for MWNTs as was measured for un-processed micro- and nanofluids. To further study the influence of particle aspect ratio on thermal conductivity, we investigated the thermal conductivity of a suspension with fixed particle volume fraction, but varying particle aspect ratio. This was done by directly reducing the particle length by additional processing of the suspensions.

Again, we started with a microfluid, containing 2.5% by volume of SiC whiskers which was processed by ball-milling to change the aspect ratio of particles. This was done in four steps, with the volume-weighted aspect ratio ultimately reduced by a factor of two from 9.6 down to 4.8, as shown in Table 4.1. The measurements of the thermal conductivity of the corresponding suspensions containing SiC whiskers of four different aspect ratios are presented in Fig. 6.1. For a fixed volume fraction, the thermal conductivity enhancement goes from 39.5 % down to 16.5% as the volume-averaged aspect ratio decreases from 9.6 to 4.8. Comparison of the experimental data

and the EMT prediction shows excellent agreement. The volume-weighted particle aspect ratio is used to predict thermal conductivity enhancement with Fricke model, *i.e.* no interfacial resistance taken into account. Again, the only other principal parameter, k_{p}, is taken to be 360 W/mK. However, it is clearly seen from the Fig. 6.1, that the calculated k is insensitive to k_{p} and fits experimental data well for the whole range of the aspect ratios for any reasonable choice of k_{p}. Note also that any possible contamination of the suspension by the grinding material itself should only increase the conductivity with grinding time, which is opposite to the observed trend. Thus, for SiC particles in the micron size range, significant differences in thermal conductivity were observed between inclusions that have different aspect ratio, but the same cylindrical shape. The volume-weighted aspect ratio was again confirmed to the correct measure to use in calculating the thermal conductivity of suspensions with anisotropic particles with a wide distribution of aspect ratios.

As for conductive heat transport in nanofluids, the Kapitza resistance should be taken into account when comparing experimental data and theoretical predictions. First, we attempted to look at recent data by Yang *et. al.* [24] in the light of effective medium theory. Yang *et al*. found that the thermal conductivity of MWNT/ poly(α-olefin)-oil (PAO) suspensions at a volume fraction of ϕ=0.0021 decreases with sonication time. They also noted that the aspect ratio of the MWNTs was decreased by the intense ultrasonication that they used. Figure 6.2, which shows Yang *et al.*'s measured thermal conductivities plotted against the nanotubes' volume-weighted aspect ratio, obtained using their reported aspect-ratio distributions, shows that there is qualitative agreement between EMT and the experimental data. Although tempting to conclude that there is quantitative agreement between EMT and the data, it should be noted that, in Yang *et al.*'s experiments the suspensions contained substantial aggregates. Furthermore, the reduction in aspect ratio with increasing sonication time was concomitant with a decrease in the size of large-scale nanotube agglomerates. Thus, it is not possible to separate the effect of decreasing particle aspect ratio from particle aggregation and other factors that may also affect the thermal conductivity. Nonetheless,

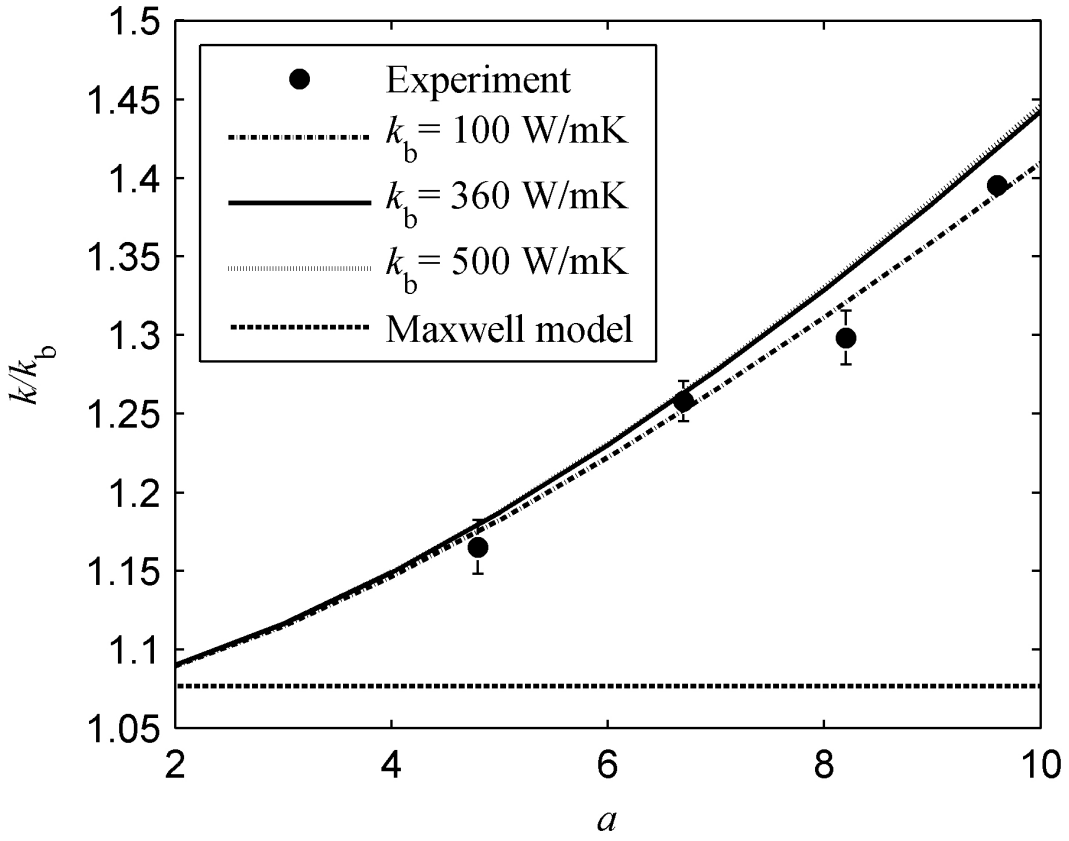

Figure 6.1: Measured thermal conductivities of 2.5% vol suspensions of SiC in EG with whiskers of different aspect ratios. For comparison, the EMT predictions for different magnitudes of k_p and Maxwell model are shown

the changes that Yang *et al.* observe in the thermal conductivity of the MWNT suspension are at least qualitatively consistent with the reduction in thermal conductivity brought about by decreasing aspect ratio that is predicted by EMT.

In order to make quantitative comparison with EMT for nanoparticle suspensions we studied a well-dispersed MWNT/surfactant and water system in which the particle aspect ratio was carefully characterized. The nanotube length was also directly varied by intense tip-sonication instead of mild bath-sonication. As the result, the aspect ratio was effectively reduced from 32.9 to 14.5 in four steps. Measured thermal conductivities of four samples containing 0.1% vol MWNTs are presented in Fig. 6.3. It can be clearly seen that the thermal conductivity enhancement of the suspension

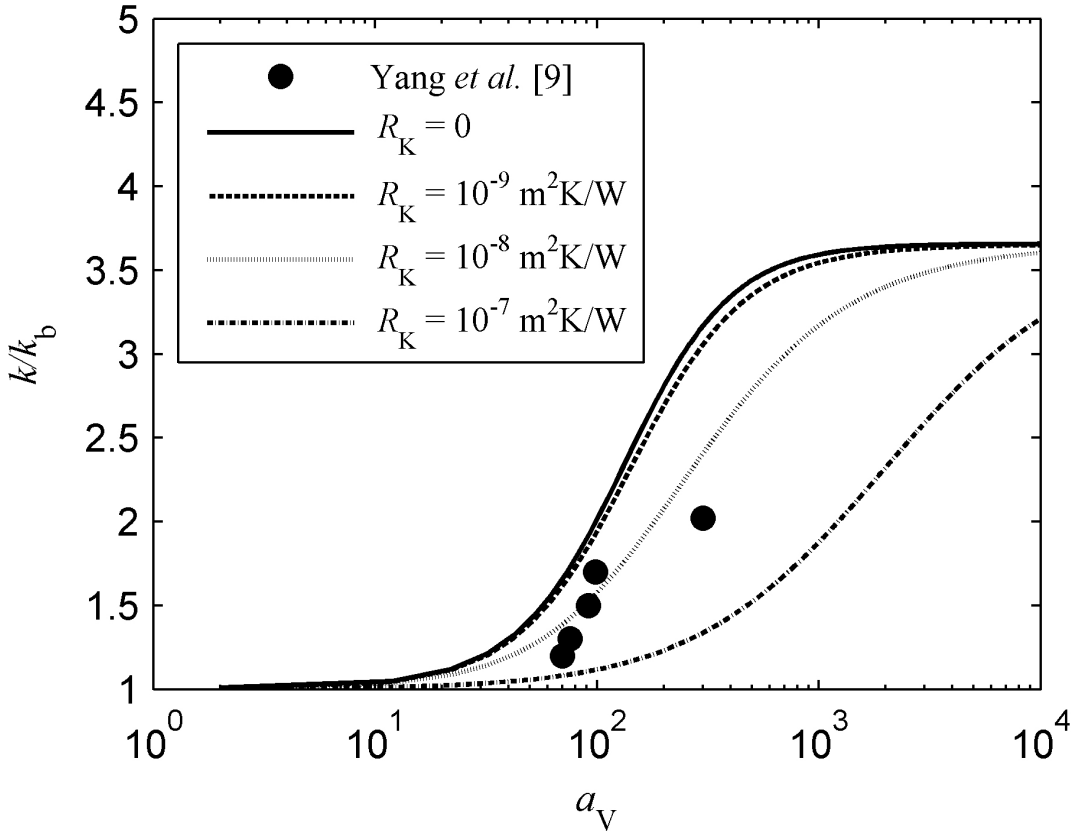

Figure 6.2: Thermal conductivities of MWNTs in PAO with different aspect ratio of nanotubes. Solid squares indicate Yang *et al.*'s measurements, while the lines show the EMT model predictions for different interfacial resistances.

dropped in half, from 8% to 4%, after the first 5 minutes of sonication. After another 10 minutes of intense ultra-sonication the thermal conductivity enhancement goes down to 1% and remains essentially unchanged afterwards. Careful comparison with EMT predictions showed that the thermal conductivity drop occurs somewhat faster than predicted with EMT. This effect could result from a decrease in thermal conductivity of MWNTs as their aspect ratio is reduced. As was discussed before, nanotube thermal conductivity depends on its length, saturating at some length. Thus, shortening the nanotubes could cause a drop in their axial thermal conductivity as well. Second, the intense sonication has been shown to damage the nanotube structure promoting an additional decrease in conductivity due to the these defects [61]. However, it is clearly

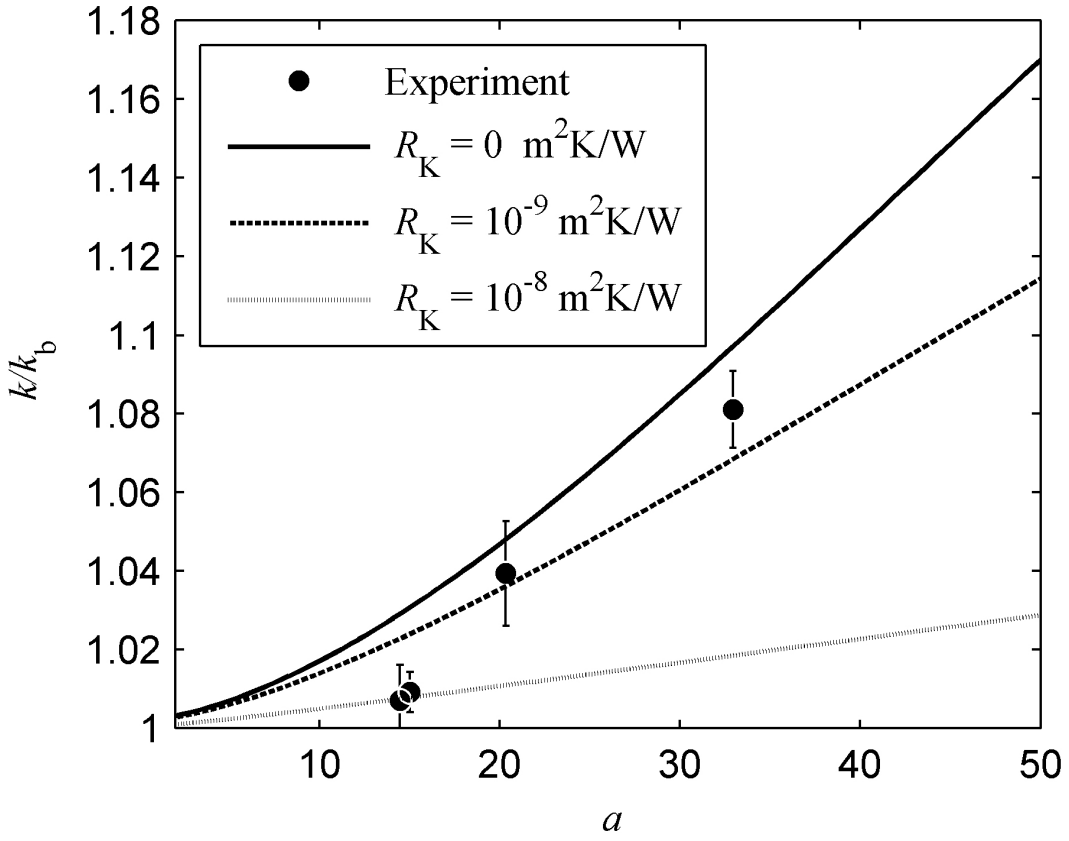

Figure 6.3: Measured thermal conductivities of 0.1% vol aqueous suspensions of MWNTs of different aspect ratios. For comparison, the EMT predictions for different magnitudes of R_{K} are shown

seen from our data that aspect ratio is a dominant factor affecting the thermal conductivity of the particulate suspensions, even for nano-sized particles such as MWNTs.

Thus, we have experimentally validated the EMT prediction that the effective thermal conductivity of suspensions is enhanced by large aspect-ratio particles. For micron-sized SiC particles, where interfacial resistance is negligible, good quantitative agreement is seen between the measured thermal conductivities and EMT for volume fractions up to 5% and volume-weighted aspect ratios ranging from 1 up to 9.6. For Yang *et al.*'s recently reported data on MWNTs in PAO, the measured thermal conductivities were qualitatively consistent with the aspect-ratio effect predicted by EMT; possible nanotube-clustering in the suspension precludes us from drawing conclusions

regarding quantitative agreement in this case. Our experiment with carefully characterized aqueous MWNTs suspensions showed that the effective thermal conductivity is a strong function of particle aspect ratio as well. The measured thermal conductivities dropped drastically as the MWNT aspect ratio was reduced in several steps by intense ultra-sonication. The experimental thermal conductivity dropped slightly faster with decreasing particle aspect ratio than predicted by EMT, possibly due to sonication-induced damage in the nanotubes. Nevertheless, our data on SiC microparticles and MWNTs doubtlessly reveal the impact of filler shape on the effective thermal conductivity of particulate suspensions.

Chapter 7

Agglomeration Stability of Nanofluids

7.1 Stability of Micro- and Nano-Suspension

The last part of the study is an investigation of connection between the agglomeration state of nanoparticles, in particular MWNTs, and the effective thermal conductivity of the suspensions. As discussed previously in Chapters 4-6, the shape of the dispersed particles is extremely important for the thermal properties of the suspension. Thermal conductivity increases in suspensions containing long fibers or tubes much more than for those with dispersed spherical inclusions. This is only true when particles are isolated one from another, however. At low concentrations, particles agglomeration and bundling can significantly reduce the *effective* aspect ratio of the suspended medium, thus reducing the effective conductivity. At higher concentrations, however, particle interactions may create a percolation path for thermal energy which would increase the effective conductivity. We propose to investigate the influence of particle aggregation on the thermal conductivity of suspensions. The thermal conductivity experiments nanofluids are coupled with measurements of agglomeration level in suspensions.

The main advantage of suspensions with nanoparticles dispersed in a liquid over the fluids containing millimeter- or even micron-sized particles is usually attributed to the their enhanced stability against sedimentation and particle aggregation. It is not always true. In general, obtaining a stable suspension of the non-agglomerating nanoparticle is the primary issue in the nanofluid research. If nanoparticles are well dispersed and separated one from another, their stability against gravitational sedimentation is very high, indeed. But particle coagulation can increase the *effective* particle size significantly and completely change the suspension characteristics, including

rheological and thermal properties.

The dispersion behavior of suspension is defined by the balance between the attractive and the repulsive forces that particles experience as they approach each other. If the attractive component is dominant over the repulsive one, particles aggregate easily, which makes the resulting nanofluid unstable. The attractive component of the intermolecular potential, or Van der Waals force, is responsible for the coagulation of nanoparticles in the nanofluids. The main part of this attractive force is the London dispersion force, which exists between any two molecules or particles and is liable for existence of the liquid itself. The dispersion force is the only attractive force in fluids containing only non-polar molecules, but other mechanisms, such as dipole-dipole or dipole-induced interactions, arise when molecules are non-symmetric. The nature of the repulsion between particles lays in the electrostatic force that exists between any two charged objects. The repulsive force is the only mechanism to prevent particles from agglomeration in fluid. The balance between these two types of interaction influences overall stability of the nanofluids [62], [63].

The quantitative measure of suspension stability is its zeta potential (ζ-potential). Each particle in colloidal suspension is charged due to its ionic characteristics and surrounded by oppositely charged ions which form the fixed layer. Outside the fixed layer, there is another layer that electrically screens the first one. This layer consists of free fluid ions of opposite to fixed layer polarities, forming a cloud-like, diffusive area. This whole area is electrically neutral and called the double layer. When the voltage is applied to a solution, particles dispersed in a liquid start moving together with surrounding fluid that is confined within an imaginary *slipping* plane which is located somewhere inside the diffuse layer. This means that the slipping plane separates mobile fluid from fluid that remains attached to the surface. The zeta-potential, which is the electrokinetic potential at the slipping plane, determines the degree of the repulsion between particles and is largely responsible for the colloidal stability of nanofluids. Typically, a zeta-potential of magnitude greater then 35 mV (either positive or negative) is sufficient to form stable suspension [62]. The principal behind measuring zeta potential is very simple. An electric field between electrodes immersed in the

sample forces particles to move toward the electrode of opposite polarity. At the same time viscous forces prevent the particle from migrating through liquid. The balance between these two forces, electrostatic attraction and the viscous drag, defines the particle velocity, or particle mobility, which is the velocity under unit field strength. Measured particle mobility is used for calculation of the zeta potential. The determination of ζ-potential is very simple for spherical particles. In the case of ellipsoidal carbon nanotubes of varying orientation distribution under external electric field we can only estimate it. However, ζ-potential data can still indicate the trend of changing the suspension stability. For more quantitative analysis of agglomeration state, we use optical absorbance measurements instead.

There are various methods to reach optimal ζ-potential resulting in stable-against-aggregation suspensions, such as varying the pH level, and different types of surface modification and treatments to particles. Among them, surfactants play an important role. Surfactant molecules, adsorbed on dispersed particles' surface, prevent them from approaching each other and aggregating. Experiments showed decrease in zeta potential of aqueous suspension of alumina from +40 mV down to -40 mV as the concentration of surfactants (Dolapix A88, 2-amino 2-methyl propanol, and Dolapix CE64, carbonic acid based polyelectrolyte) increased [64]. The optimum concentration of NaDDBS for 0.1% copper nanosuspensions was found to be 0.07% by mass, 0.43% for TX-10 and 0.05% for CATB [65]. This effect can be explained with the example of NaDDBS. In a neutral aqueous medium, copper nanopowder is charged positively, so anionic phenyl sulfonic group dissociated from NaDDBS is adsorbed at the particle surface. The net surface charge becomes negative and increases as the surfactant concentration increases. This means that more anionic groups are pushed into surrounding nanoparticle double layer. But the concentration of positively charged Na^+ groups increases as well and, at some point, the Na^+ groups start entering the electrical double layer resulting in a decrease of electrostatic repulsive force between particles.

Dispersion characteristics are extremely important for understanding suspension

thermal and rheological properties. Those properties depend significantly on the degree of particle agglomeration. Some of the reported recently particle-size measurement have revealed that agglomerate size distributions in dispersions are in a good agreement with data on particle zeta-potentials [66, 67]. The maximum agglomerate size in a suspension strongly correlates with its isoelectric point (IEP). Recent experiments showed that degree of agglomeration had a great effect on viscosity of suspension containing alumina. The variation of a particles size is reflected in a viscosity change. Measurements revealed a well defined maximum peak in viscosity of aqueous alumina suspension near corresponding to its minimum colloidal stability [66]. Although no experimental data available for dispersion characteristics effect on thermal conductivity, it is expected to be similar to the effect observed for rheological properties in suspensions.

The important task of producing a stable nanofluid becomes more challenging when it comes to suspensions containing carbon nanotubes. Carbon nanotubes, both multi-walled and single-walled, are hydrophobic in nature and usually exist in bundles. The outer diameter of MWNTs is about tens of nanometers and do not exceed few nanometers for SWNTs. At the same time nanotubes have very high aspect ratio, which makes them bend easily and aggregate not just into the bundles, but into the agglomerates of different sizes and shapes. The electrokinetic behavior of CNTs in water is defined by electrostatic interaction between carbon atoms, and in that way it is similar to the properties of carbon black aqueous dispersions. Carbon black nanoparticles have very low dispersibility in water at mild pH values near the isoelectric point of carbon, which occurs at pH 6 [67]. The particles are negatively charged at pH above the isoelectric point and positively at pH values below 6. The zeta-potential of single-walled carbon nanotubes was measured to be close to that of carbon black spherical particles and has its IEP at pH 7 [68]. This means that when carbon nanoparticles or nanotubes dispersed in neutral water, agglomeration occurs very fast and the suspensions are unstable.

To achieve high stability of CNTs suspensions in water the nanotube surface charge should be controlled. Different types of surface modification are employed to stabilize

(a) Surfactant to nanotube mass ratio of 5X

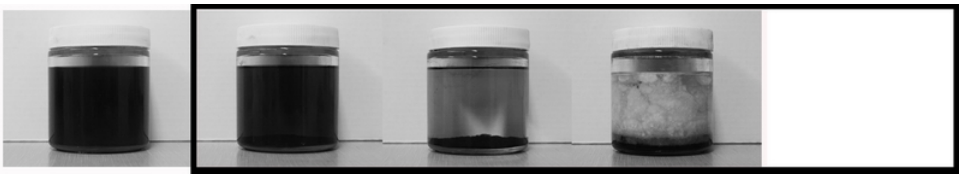

(b) Surfactant to nanotube mass ratio of 100X

Figure 7.1: Nanofluids 1 week after preparation. MWNTs volume fraction are 0.01%, 0.02%, 0.05%, 0.1% and 1%.

CNTs dispersions along with addition of the surfactants. Among them are addition of surfactants or dispersants [69], [51], nitric-acid surface treatment [70], [71], polymerization [72], controlling pH level [73], [74], etc. In this study we investigated how surfactant concentration and its ratio relative to the mass of CNT influences the stability of MWNT nanofluid. Among the most widely used surfactant we mark out sodium dodecyl sulfate (SDS) and sodium dodecylbenzene sulfonate (NaDDBS, or SDBS). These are the most common surfactants used in aqueous carbon nanotubes suspensions and have proven to be highly effective in dispersing CNTs. Even though both of them are considered to be good dispersant, NaDDBS was shown to be more efficient [51]. Islam et al. reported that $\sim 63\%$ of SWNTs were individualized in aqueous NaDDBS suspensions for CNT concentrations as high as 20 g/L ($\sim 1\%$ volume fraction), and that those suspensions remained stable much longer than those containing sodium dodecyl sulfate or Triton X-100. Islam et al. also found an optimal surfactant-to-CNT mass ratio (SCR) of 10:1 that resulted in stable suspensions for over 3 months at concentrations up to 20 g/L.

In our aqueous suspensions with nanotube volume fractions ranging from 0.1% up to 1%, we observed good stability in all samples with NaDDBS concentration below $\sim$ 20g/L. No aggregation or sedimentation was detected in these samples during the

period of few weeks (Figure 7.1). However, above a critical NaDDBS concentration of approximately 20-50 g/L, sedimentation occurred regardless of the nanotube volume fraction. This is seen in Fig. 7.1, which shows images of suspensions containing 0.01% to 1% of MWNTs and surfactant mass ratios 5X and 100X. It is clearly seen that sedimentation occurs in samples with different nanotube volume fractions but at the same critical concentration of surfactant. For suspensions containing 5 times more surfactant than NTs by weight, good stability is observed for a sample containing 10 g/L of NaDDBS. This concentration corresponds to a CNT volume fraction of 0.1%. Partial sedimentation starts at a surfactant concentration of 25 g/L (0.25 % vol of CNTs) for all suspensions at SCR 5X. As shown in Fig 7.1 samples containing 100 g/L of NaDDBS (1% vol of CNTs) are completely sedimentated after few hours. For suspensions of SCR of 100X, ϕ=0.01 is the maximum volume fraction of nanotubes for stable suspensions. Again, this corresponds to a surfactant concentration of 20 g/L. Thus, we observed nanotubes sedimentation in all samples containing surfactant at 20 g/L and above. At very high NaDDBS concentrations ($\sim$ 100 g/L) not only do nanotubes aggregate and fall down, but surfactant flakes fall from the suspension. Samples with NaDDBS fraction below 20 g/L remained stable during the observation time of several weeks with only insignificant amount of sediment on the bottom.

The critical concentration of NaDDBS at $\sim$ 20 g/L is believed to be attributed to a phase transition in the MWNT-NaDDBS-water system. For a two-component NaDDBS-water system the Krafft point is reported to be at 27.6 ^{o}C [75], which is higher than our experimental temperature of 20 ^{o}C. This may explain the lack of surfactant micelles observed visually, even though the surfactant concentration is far above critical micelle concentration (CMC) for NaDDBS in water (reported to be 0.45 g/L [76]). A similar absence of micelles was reported by Islam *et al.*, who observed no micelles forming in their aqueous suspensions [51]. However, the presence of nanotubes, or any other additive, can shift the Krafft point. The micelles were reported to present in NaDDBS/water systems in presence of cetyltrimethyl-ammonium tosylate (CTAT) at NaDDBS concentration of least up to 50 g/L [77] at temperature of 25 ^{o}C, which is below the Krafft temperature for pure NaDDBS-water systems. Our experimental results

also indicate that some kind of transition occurs in suspensions at NaDDBS fraction of 20-50 g/L. Although no detailed phase diagram is available for the NaDDBS-MWNT-water system, we believe this critical NaDDBS concentration corresponds to a transition between different phases of NaDDBS. It is expected to be similar to the phase diagram of other surfactants, SDS, for example, where a micelle regime that extends up to 40% wt at higher temperatures and is followed by hexagonal phase with more complicated surfactant structure or mixed regimes [78]. This kind of transition might explain the critical volume fraction of NaDDBS of approximately 20-50 g/L that we observe in the MWNT suspensions.

Table 7.1: Measured ζ-potential of NaDDBS-stabilized MWNTs suspensions

NaDDBS fraction, g/L	Measured particles's mobility, $\frac{\mu/\mathrm{sec}}{\mathrm{V/cm}}$	ζ-potential, mV
20	-4.83	-61.81
50	-4.71	-60.29
100	-1.88	-24.10
200	2.68	34.29

In order to describe the degree of agglomeration quantitatively, visual observation is not enough. However, direct measurement of inter-particle zeta-potential for MWNT suspensions is complicated, since the relation between particle mobility and zeta-potential depends on particle size, shape and orientation, among other things. For spherical particles this relation is well-known. However, we attempted to estimate qualitatively stability of MWNT suspensions of varying surfactant concentrations using a ZetaPALS zeta potential analyzer (Brookhaven Instruments Corporation, Holtsville, NY), which utilizes Smoluchovsky Equation for calculating zeta potential. Measured particles mobility and zeta-potentials for suspensions containing 20-200 g/L of NaDDBS are shown in Table 7.1. Zeta-potentials were calculated assuming spherical shape of dispersed particles, which is not appropriative for nanotubes. Nevertheless, it is clear that absolute magnitude of ζ is decreasing with increase of the surfactant concentration at low concentration of surfactant and afterwards passes through its isoelectric point. Than the ζ is increasing, but obviously not high enough

for suspension to be stable. Though, we conclude that suspensions become more and more unstable as concentration of NaDDBS increases above 20 g/L. This result is consistent with visual observation of suspension stability and the thermal conductivity measurements that will be discussed later. However, this result can be only considered a qualitative indicator that an excessive amount of surfactant is not promoting better dispersion of CNTs in water.

The quantitative analysis of the sedimentation dynamics can be performed with the means of another optical method widely used for analyzing properties of liquid suspensions. This approach in characterizing the degree of agglomeration in nanofluids is based on light absorption phenomenon in suspensions. Absorbance of liquids is usually defined as [79]

$$A = -log\frac{I}{I_0} \tag{7.1}$$

where I and I_0 are transmitted and incident light intensities correspondingly. In general, the absorbance of a base fluid, especially water with dissolved surfactant, is not zero. Since we are interested in absorbance only due to MWNTs dispersed in suspensions, our absorbance data are normalized by the transmitted light intensity of corresponding base fluid (surfactant and water), not the incident light intensity. According the Beer-Lambert law absorbance is linearly proportional to the molar concentration of dispersed particles, c:

$$A = \epsilon l c, \tag{7.2}$$

where, ϵ is a molar absorptivity of the absorber and l is the absorption path length. Since absorbance is proportional to the concentration of absorbing species, the measurements of the amount of light that has passed through a sample give us information about any changes in the amount of particles dispersed in liquid. In practice, Eq. 7.2 holds for $A \approx 1$, since at higher absorbances the dependence between the absorbance and the concentration can become non-linear due to inter-particle interaction, *i.e.* shading effects. Monitoring absorbance in real time gives us the information about

concentration of the dispersed particles. Samples that are stable against bundling and sedimentation should have constant absorbance. For unstable samples, the absorbance should drop gradually until zero. The amount of time needed for suspension to clear up from any agglomerates is defined by the average aggregate size. Using Stokes law for sedimentation time, defined as

$$t = \frac{4.5\mu L^*}{(\rho_{\mathrm{p}} - \rho_{\mathrm{b}})gr^2}, \tag{7.3}$$

where L^* is characteristic scale, g is gravity, μ is viscosity of a base fluid and ρ_p and ρ_b are the densities of the dispersed and dispersing phases, respectively, we obtain the average agglomerate size in water to be around 200 microns if a sedimentation time is 4 sec for a 10-cm in tall vial.

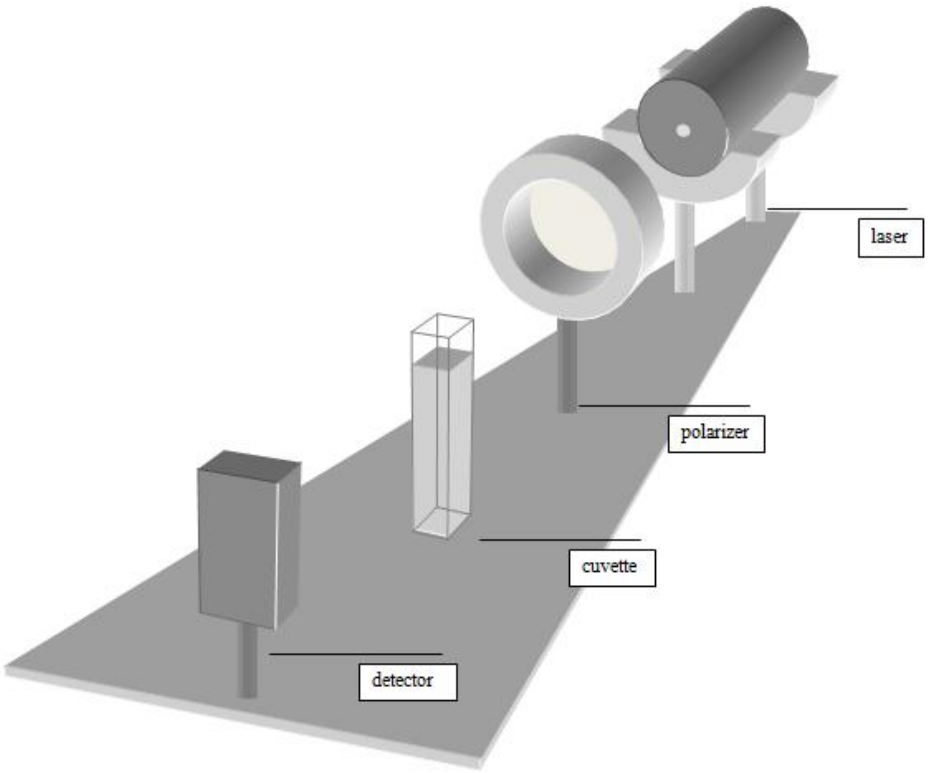

Figure 7.2: Experimental setup for absorbance measurements

In our experimental setup the beam of a helium-neon laser was passed through a sample housed in a glass cuvette and incident on a photodiode (Fig. 7.2). Measured light intensity was used to calculate the absorbance. The cuvette with path length of only 1 mm allowed to use original (non-diluted) suspension with 0.1% volume fraction of nanotube. We monitored absorbance during 24 hours for sample with surfactant to NTs mass ratio of 10X. As discussed above, this suspension demonstrates very good visual stability against sedimentation and a significant increase in thermal conductivity. The suspension remained stable during the observation time of a few weeks and no discernible sedimentation occurred during this period. It can be clearly seen in Fig. 7.3 that absorbance approaches a plateau after short initial decay. The plateau absorbance is about 80% of the initial absorbance which corresponds to approximate $\sim 20\%$ drop in the nanotube concentration. This is a rough estimate of the concentration change according the Beer-Lambert law which postulates that absorbance is linearly proportional to the molar concentration of dispersed particles only up to $A \simeq 1$. However, the initial decrease in absorbance allows us to assume that some agglomeration still occurs in the suspension during the first two hours. Nevertheless, we can conclude that nanofluid containing 0.1% of MWNTs by volume is very stable since the absorbance remains constant for another 22 hours once it reaches a plateau after a short initial decay. Again, further visual observations indicated that suspension is stable for the period of few weeks.

Absorbance data, ζ-potential estimate and suspension-stability visualization are in a good agreement with the thermal conductivity data presented in Fig. 5.3. It can be clearly seen that stable suspensions, which contain well-dispersed and mostly individualized particles, are capable of the highest thermal conductivity enhancements. For all nanofluids, the thermal conductivity increases with volume fraction of NTs until the surfactant concentration reaches it critical magnitude of about 20-50 g/L. As a result, we see the longest linear regime for suspensions with SCR 5X and 10X, and there is almost no linear trend for nanofluid at 100X. This linear regime corresponds to the well-dispersed stable fluids with a high fraction the individualized nanotubes. Only

long individual nanotubes enhance the thermal conductivity of suspensions significantly. On the contrary, suspension containing clumped and aggregated nanotubes, can be interpreted as suspension containing large, almost spherical particles (agglomerates). However, these agglomerates do not contribute much in thermal conductivity, as seen in Fig. 5.4 for surfactant concentrations above ~ 20 g/L.

In summary, we found sodium dodecylbenzene sulfonate to be an effective in dispersing MWNTs in water for NaDDBS concentrations up to 20 g/L. At higher concentrations, the surfactant destabilizes the nanofluid causing a drop in the thermal-conductivity enhancement. The optimal surfactant-to-nanotube mass ratio yielding the highest thermal conductivity enhancement was found to be 10X. It should be noted though that the fact that optimum surfactant concentration is the same as that reported by Islam *et al*. for SWNTs is most likely a coincidence [51]. This parameter likely depends on nanotube properties, such as type (MWNT vs. SWNT), diameter, etc, and the nanotubes used in this study and by Islam *et. al.* are different.

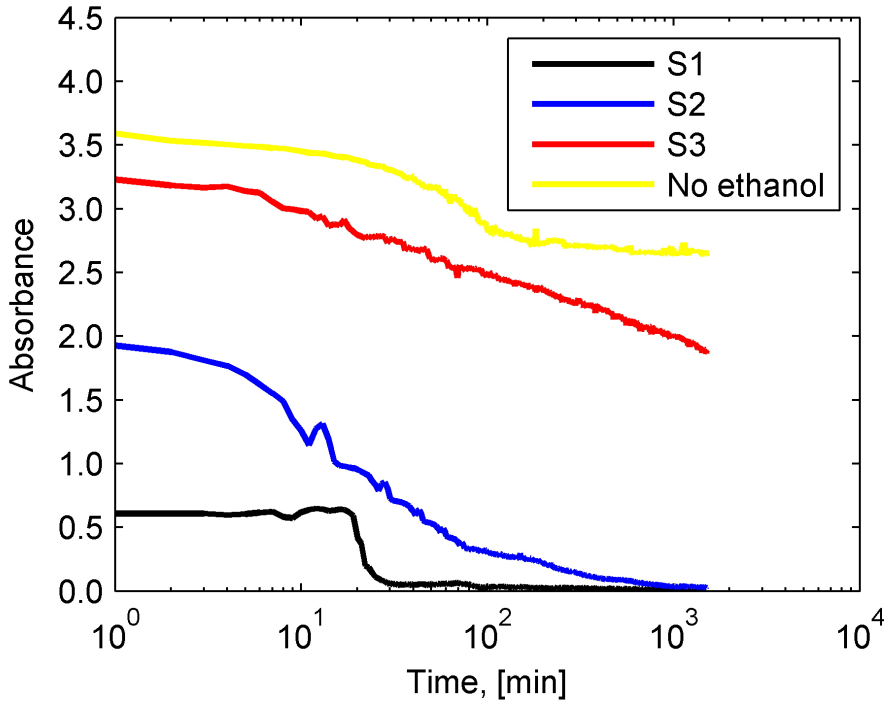

Figure 7.3: Absorbance of MWNTs aqueous suspensions for varying amount of added ethanol.

7.2 Ethanol De-Stabilization of Nanofluids

The majority of surface modification methods are aimed to obtain nanotubes that tend to repel from each other. Addition of different surfactant, polymer wrapping, etc. introduce additional molecules or particles on the CNTs surface. However, some technical applications, *e.g.* electrical, require nanotubes to stay clear of any additives. Different techniques are utilized to obtain CNTs free of any surface impurities. For instance, ethanol and methanol are widely used for removing the surfactant residuals adsorbed on nanotube surface. Experiments by Zhang *et al.*, aimed to investigate the effectiveness of the different CNTs' surface cleaning procedures in order to improve the electrical contact between nanotube and the electrode in CNT field effect transistors (CNTFETs), showed complete removal of SDS residual from SWNT surface by mean of the ethanol immersion [80]. Desorption of the surfactant from the nanotubes after addition of alcohol promotes the aggregation of nanotubes into bundles. Eda *et al.* observed a decay in absorbance starting from top of the measurement vial after methanol was added to aqueous suspension of SWNTs [81]. According to Eda *et al.*, this type of absorption behavior demonstrates that bundling takes place immediately upon the addition of de-stabilization agent, even though absorbance at a given height remains constant for up to some time. This is a time needed for agglomerates to gain a critical mass and start settling below the level of the absorption measurement. After precipitation of the bulk of the nanotubes, the absorbance becomes zero throughout the vial.

To investigate the effect of agglomeration in NaDDBS stabilized aqueous suspension of MWNTs further, we attempted to de-stabilize a well-dispersed suspension of MWNTs by adding varying amount of ethyl alcohol. Afterwards, we compared the thermal and sedimentation behavior of the nanofluids with and without addition of ethanol. Several suspensions were obtained by diluting aqueous nanofluid (E0) at 20 g/L mass fraction of NaDDBS with ethanol. Volume fraction of nanotubes was maintained constant at 0.1% for all suspensions. Before addition of ethanol all suspensions showed no significant sedimentation, which was confirmed by measuring

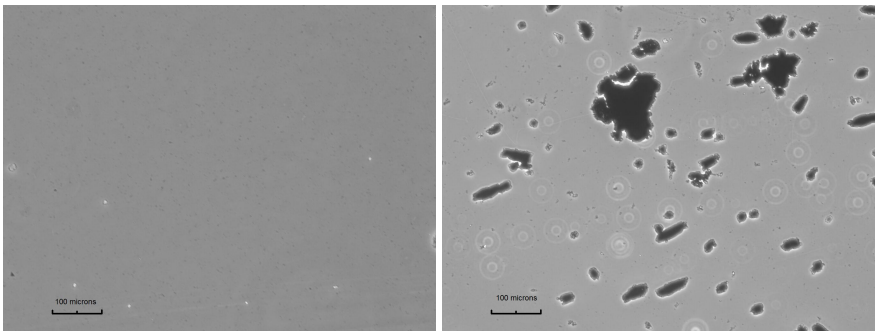

(a) x10

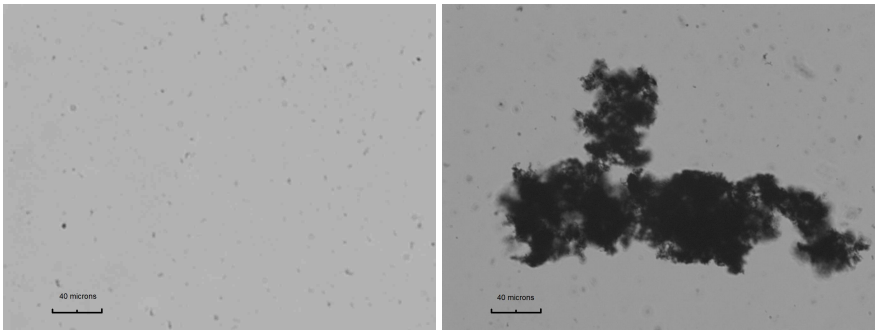

(b) x40

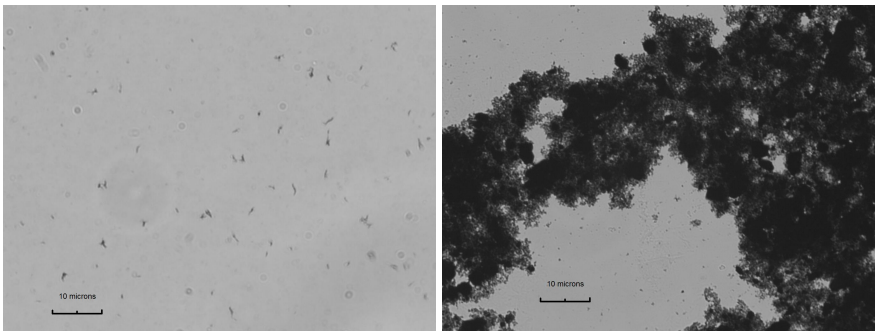

(c) x100

Figure 7.4: Optical micrographs of 0.1% MWNT suspensions, aqueous (on the left) and diluted with 1 part of ethanol per 1 part of water (on the right) at different magnification

the absorbance. After mixing the base nanofluid with ethanol at 1:1 (E1), 2:1 (E2) and 3:1 (E3) ratios, the light absorption experiment showed that intense agglomeration of the dispersed nanotubes into bundles and aggregates occurred after ethanol de-stabilization. As shown in Fig. 7.3 the most rapid agglomeration occurs in the nanofluid containing the largest fraction of ethanol (E1). It can be clearly seen that for the suspension containing 50% ethanol by volume (E1) the aggregation and sedimentation of solid content starts almost immediately. Optical micrographs (Fig. 7.2) of the E1 nanofluid, taken 10 minutes after addition of ethanol, reveal that majority of nanotubes are aggregated into massive agglomerates with size up to 200 microns. Simple visual observation show that agglomeration starts immediately after ethanol was added. Due to the very large size of aggregated objects, sedimentation occurs very fast. For comparison, optical micrographs of the original 0.1% vol suspension (E0) are shown in Fig. 7.2 also. Some negligible amount of agglomerates still present in the sample, but the size of agglomerates does not exceed few microns. However, the sedimentation of these small aggregates cause a slight decrease in absorbance as seen in Fig. 7.3 for E3 and the no-ethanol suspensions E0. Intense agglomeration is taking place in suspensions E1 and E2 during the observation time with no sign of reaching a plateau as for original nanofluids. The slopes of the absorbance curves result from sedimentation behavior of large agglomerates. As shown in Fig. 7.3 particle settling starts some critical time after addition of ethanol, which means this is the time needed to form agglomerates heavy enough to sink down. Then we see almost exponential decay in absorption. This result is in agreement with the classical sedimentation Mason-Weaver theory for sedimentation of small particles under a gravitational force [82]. It takes around 20 minutes for E1 suspension to clear up completely. Full sedimentation in E2 requires time of around 16 hours. Suspensions E0 and E3 still contain dispersed particles after 24 hours of absorbance measurements.

Next, we conducted thermal conductivity measurements of ethanol-destabilized nanofluids in real time along with evaluation of their dispersion characteristics. Absorbance measurements were coupled with thermal conductivity experiment for all four sample with and without ethanol. Measurements started 10 minutes after the

ethanol was added and were re-iterated every 10 minutes for the first three hours. Additional 5 measurements were taken 24 hours after additions of ethanol.

It can be seen from Fig. 7.5 that thermal conductivities remain stable for all suspensions during the observation time. This result together with absorbance data and optical micrographs analysis show that ethanol causes desorption of the surfactant right after it is added. After surfactant is removed from nanotube surface very fast nanotube aggregation occurs followed by slow sedimentation. A constant thermal conductivity during this time means that the amount of agglomerates remains the same over time, since non-elongated aggregates do not contribute much in the suspension thermal conductivity compared to long individualized nanotubes.

For the suspension E1 diluted with 50% of ethanol no increase in thermal conductivity over that of the base fluid (ethanol-water-surfactant) was observed. For this suspension it is clearly seen from the optical micrographs in Fig. 7.6 that aggregated nanotubes settle down completely in 10 minutes after addition of ethanol. This result is in agreement with no noticeable increase in E1 thermal conductivity. For the suspension E2 containing base nanofluid and ethanol at ratio 3:1 the average thermal conductivity increase is 6.8%. This is close to the thermal conductivity enhancement in well-dispersed aqueous suspension with no ethanol added, which was 8.6% when averaged over 24-hours period. The increase in thermal conductivities of E2 and E3 means the amount of ethanol is not enough to strip down the adhered surfactant molecules from all nanotubes. At the same time smaller increase in thermal conductivity (4.6% and 6.8% correspondingly) shows that some surfactant desorption occurs in these suspensions.

It should be noted also that the time scale for absorption and conductivity measurements is different due to the difference in a fluid height in the optical-absorption cuvette and the thermal-conductivity testing vial. According to Stokes law, the sedimentation time is proportional to the height, h. For instance, complete sedimentation in E1 occurs about 20 minutes after addition of ethanol as shown in Fig. 7.3. Visual observation of thermal-conductivity-testing vial gives a sedimentation time of around 1 hour, which is consistent with this vial's greater height compared to the size of the

absorption-testing vial. Using Stokes law, we estimate average size of the aggregate to be 6 microns. This means that first 6 data points presented in Fig. 7.5 for E1 were taken when some agglomerates were still suspended in a liquid, followed by complete CNTs sedimentation. However, thermal conductivity remained essentially unchanged, which allows us to conclude that the fraction of individualized nanotubes that contribute the most in thermal conductivity increase is negligible. The fact that thermal conductivity do not change significantly for all samples means that the initial agglomeration occurs immediately after addition of ethanol, and after that the amount of individualized CNTs remains constant.

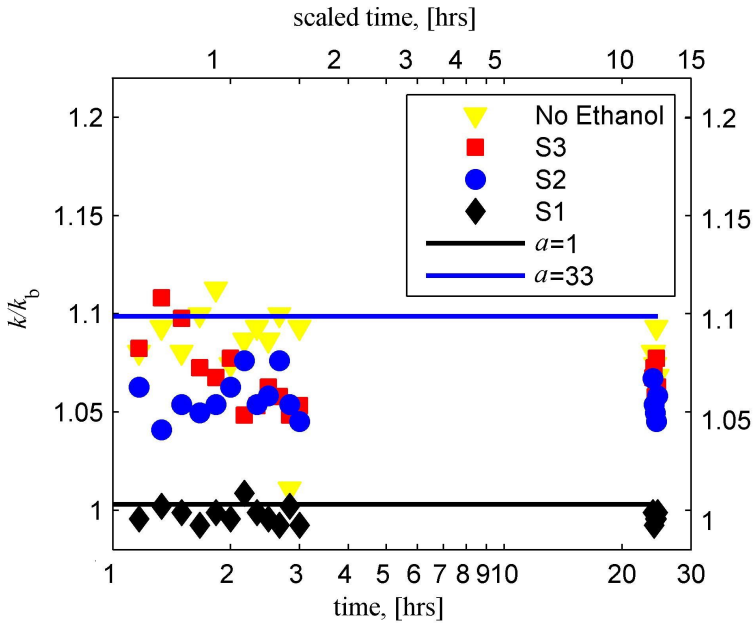

Figure 7.5: Thermal conductivities of MWNT aqueous suspensions for varying amount of added ethanol. Real time is shown on the lower horizontal axis, while time scaled to time of the optical absorption experiment is shown on the upper axis

(a) no ethanol added

(b) S3 (3:1 base fluid to ethanol)

(c) S2 (2:1 base fluid to ethanol)

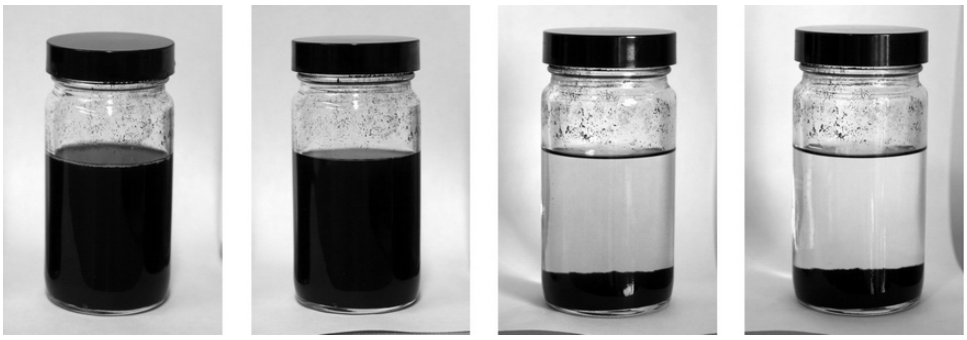

(d) S1 (3:1 base fluid to ethanol)

Figure 7.6: Sedimentation of nanotubes in suspensions at different fraction of ethanol 1 hour, 3 hours, 1 day and 1 week after mixing with ethanol.

Chapter 8

Conclusions

In this study the effects of particle aspect ratio and agglomeration state in liquid suspensions of micro- and nano-particles were investigated. The experimental data were analyzed in the light of Maxwell/Fricke/EMT predictions that the thermal conductivity of a composite material can be significantly enhanced by addition of a small amount of highly conductive particles, especially those with high-aspect ratio. To test the theory in real experiments, in which particles typically have a broad length distribution, we showed that the volume-weighted aspect ratio is the correct measure to use in the Fricke/EMT equations. In order to find such volume-averaged aspect ratios in real suspensions, particle distributions can be measured from optical or TEM micrographs. Also, it was shown that the thermal conductivity of the dispersed phase, or the thermal-conductivity ratio, δ, has no or a little effect on the effective conductivity, k, if δ is high enough. This is an important result, since reported thermal conductivities for CNTs as well as for SiC are in a wide range and depend on many other properties. Using the Bruggeman approach, some theoretical analysis was carried to test the validity of the Fricke/EMT equations in the light of possible particle thermal interaction. It was shown that inter-particle thermal interaction is unlikely to be responsible for conductive-heat-transport enhancement at such low volume fractions of dispersed particles.

Our experimental data on both nano- and micro-sized particles dispersions showed a good agreement with classical theory provided that volume-averaged aspect ratio is used for calculations. For SiC particles the comparison was made with macro-scale Maxwell/Fricke theory with no interfacial resistance taken into account due to the large size of the particles. Data from the experiments on MWNT dispersions showed

a good agreement with effective medium theory providing a low but still reasonable magnitude of the interfacial resistance is used in calculations.

Experimental data on both micron-sized SiC particles and nano-sized MWNTs doubtless revealed the impact of filler shape on the effective thermal conductivity of particulate suspensions. Measurement performed in micro-fluids containing spherical and cylindrical particles showed the significant difference in their thermal conductivity enhancement. To investigate the effect of particle shape further, thermal conductivity measurements were performed for particles of different aspect ratio. This was achieved by varying the length of the particles suspended in fluid via additional processing of both nano- and micro-suspensions. Grinding the SiC suspension in a ball milling machine reduced the aspect ratio of the whiskers by the factor of two in several steps. Nanofluids were processed in high-power tip sonicator, and the nanotubes were also shortened almost in half. Careful analysis of particle geometry was carried out for every sample by optical and TEM imaging, and the volume-weighted aspect ratio was calculated at every step along with thermal conductivity measurements. Excellent agreement with Fricke predictions was observed for micro-suspensions of cylinders with aspect ratios different by the factor of two. For the MWNT suspensions, the experimental data was found to be in a reasonable agreement with theory providing that the Kapitza interfacial resistance is taken into account. Despite a slight discrepancy of measured data and theoretical predictions for nanofluids, the impact of filler aspect ratio on thermal conductivity was validated experimentally for suspensions with large fractions of long, individually dispersed particles.

Finally, the agglomeration state of MWNTs is shown to have a profound effect on conductive heat transfer in nanofluids. To analyze the aggregation state of the suspensions, a combination of visual observation, ζ-potential measurements and optical-absorbance measurements were utilized. Carbon nanotubes were dispersed in water with the aid of sodium dodecylbenzene sulfonate and it was shown that the degree of aggregation in the nanofluids increases with surfactant concentration. The ζ-potential is negative at low NaDDBS volume fraction, then it gradually increases and passes through its isoelectric point, becoming positive afterwards with increasing surfactant

concentration. Even though this is only qualitative result, it is in a good agreements with thermal conductivity data and visual stability observation. For thermal conductivity data, we mark out two regimes of the conductivity enhancement. The initial linear increase in conductivity with CNTs volume fraction is associated with regime of nanofluid stability. This is the regime where we see good agreement between our experimental data and theoretical predictions. It is hold up NaDDBS concentrations of around 20-50 g/L and does not depend on surfactant-to-nanotube mass ratio in the 5X-100X range. The optimum ratio was found to be 10X, which yielded the largest thermal conductivity enhancement and good stability in a wide range of CNTs concentration. The following drop in thermal conductivity enhancement for NaDDBS concentrations greater than 20 g/L corresponds to poor sedimentation stability of the samples. The very low fraction of individualized nanotubes in these suspensions means that their thermal conductivity can not be described in the light of EMT.

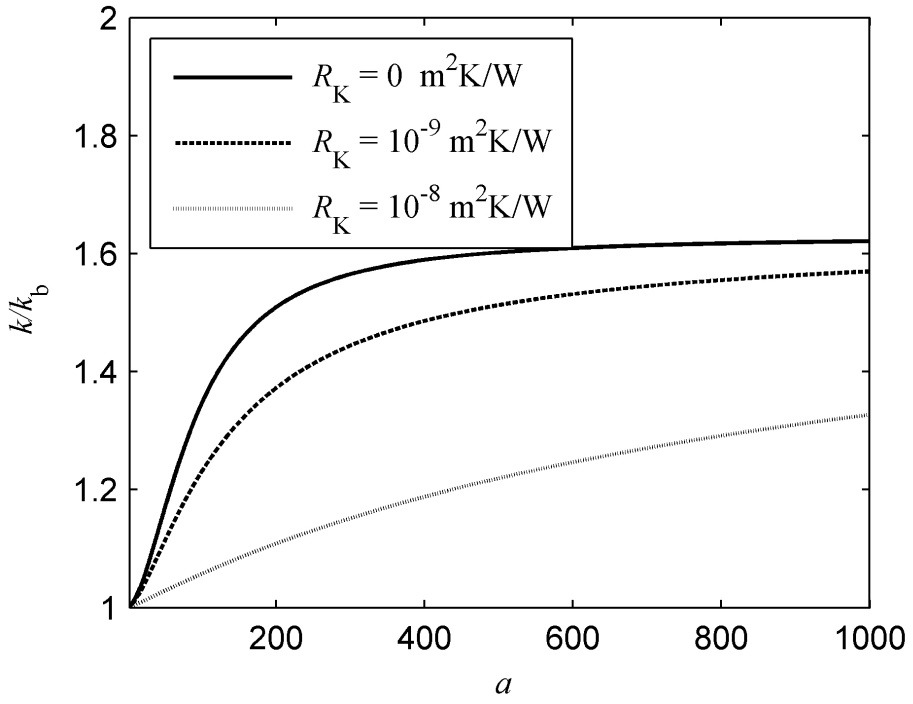

Figure 8.1: EMT calculations of the expected thermal conductivity increases for a 0.1% vol aqueous suspension of MWNTs of varying aspect ratio, assuming k_p=1000 W/mK.

The effect of aggregation on sedimentation stability and thermal conductivity of MWNTs dispersions was demonstrated further by de-stabilizing previously stable nanofluids by addition of ethanol. Suspensions were diluted with varying amount of ethyl alcohol, which can strip out the surfactant molecules from the nanotube's surface and is usually used as a cleaning agent. The aggregation of MWNTs in nanofluids with fraction of ethanol from 0% to 50% was studied. It was shown that increasing amount of ethanol promoted more intense surfactant desorption from nanotube surface and resulted in less suspensions stability. Thermal conductivity measurements coupled with optical absorbance experiment indicated that surfactant is removed from MWNTs almost immediately after addition of ethanol, followed by nanotube aggregation and slow sedimentation of agglomerates. Thermal conductivity data confirmed that only individualized particles contribute in total thermal conductivity of composite fluid and that the agglomeration state of MWNTs suspensions has a great influence on their thermal conductivities.

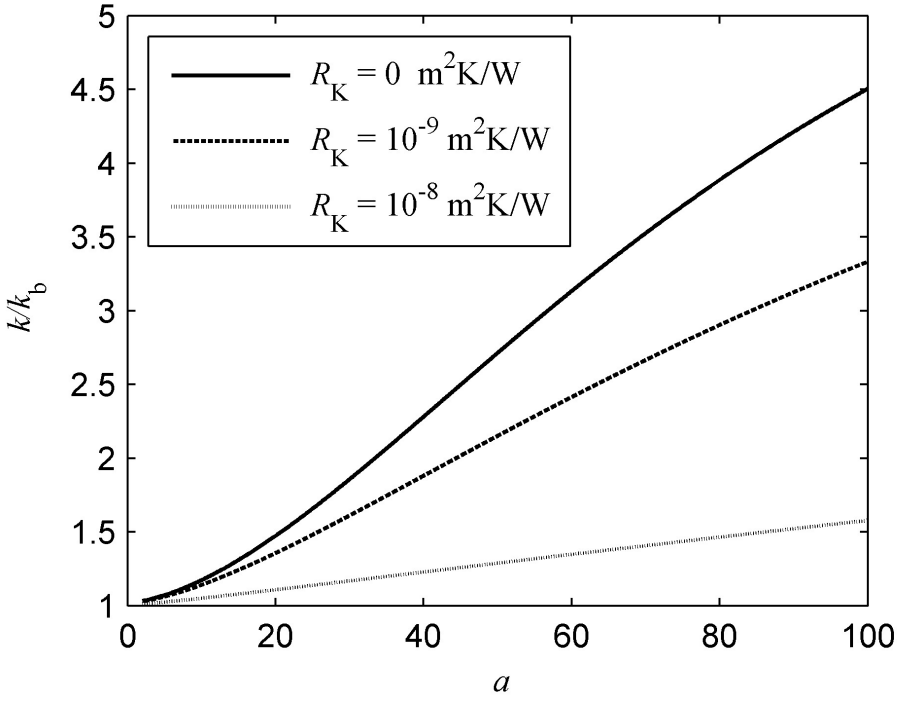

Figure 8.2: EMT calculations of the expected thermal conductivity increases for a 1% vol aqueous suspension of MWNTs of varying aspect ratio, assuming k_p=1000 W/mK.

Based on the work detailed in this thesis, we can assess the possibility of developing a nanofluid having a substantially enhanced thermal conductivity. An increase in thermal conductivity far above the maximum enhancement of 8% found in the current work, could result from some combination of 1) Higher particle aspect ratio, 2) Higher particle volume fraction, 3) Particle alignment, and 4) Particle chaining (percolation). Using carbon nanotubes as the solid phase, and keeping the solid volume fraction at 0.1%, effective medium theory predicts that nanotubes of aspect ratio ≈ 500 would be required to provide a 50% increase in the thermal conductivity of water (Fig. 8.1). However, this is the maximum possible increase in thermal conductivity in an aqueous, well-dispersed, non-percolated suspension of MWNTs at 0.1% vol, providing the thermal conductivity of the nanotubes is $k_{\mathrm{p}} \approx 1000$ W/mK. An increase in the thermal conductivity of nanotubes through the reduction of the their diameter or usage of SWNTs could possibly lead to further heat transfer augmentation in such suspensions. If the maximum volume fraction of nanotubes in suspension could be stably increased to 1%, then an aspect ratio of only 50 would be sufficient to double the thermal conductivity as seen in Fig. 8.2. This aspect ratio is very close to the aspect ratio of the nanotubes used in present study. However, more efficient dispersing techniques would be required in this case to obtain the nanofluid with such a high fraction of individualized tubes, since the NaDDBS used in this study was shown to be effective only up to mass concentration of 20g/L. Particle alignment, which can be induced by shear flow [83], [84], [85], electric fields [84], [86], [85] or magnetic fields [87], [88], [89] would also increase the thermal conductivity. Alignment can be easily taken into account by replacing depolarization factors $f^{(\mathrm{x})}$ with $f^{(\mathrm{z})}$ in Eqs. 2.14, 2.27. As seen in Fig. 8, the thermal conductivity of a 1% vol suspension of carbon nanotubes of aspect ratio 100 would increase by $\approx 60\%$ if the nanotubes were aligned by some means. At higher volume fractions and aspect ratios of nanotubes, a tripling in thermal conductivity enhancement is theoretically possible in aligned suspensions compared to those containing randomly oriented nanotubes.

Finally, percolation, which can be induced by magnetic or electric-field induced dipolar interactions between nanotubes, could further increase the conductivity of the

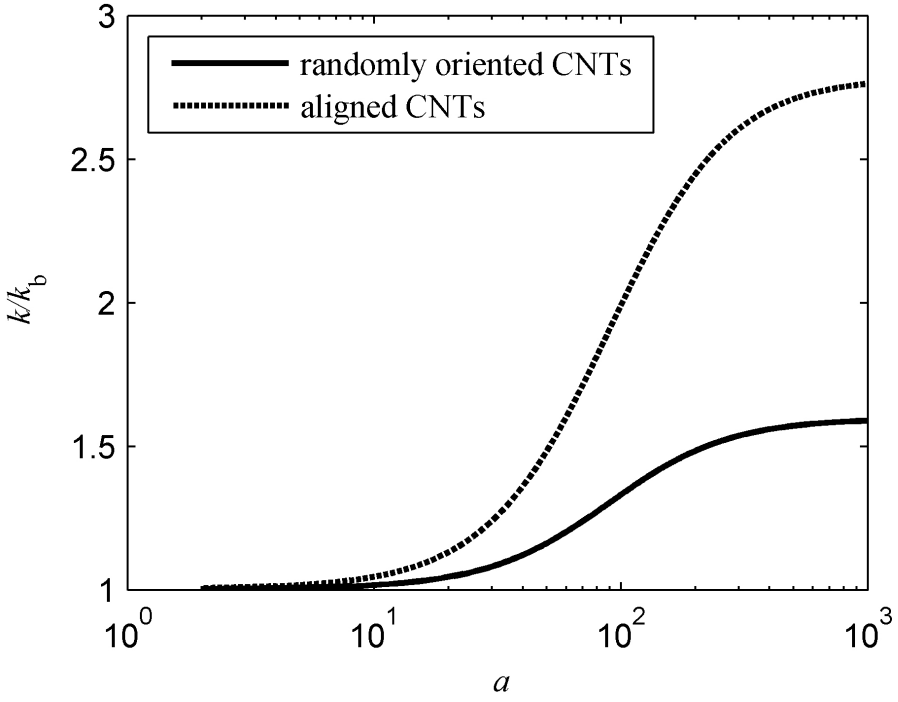

Figure 8.3: Calculated thermal conductivity increases for 1% vol aqueous suspensions of aligned and randomly oriented MWNTs, assuming k_{p}=1000 W/mK and $R_{\mathrm{K}} = 10^{-9}\mathrm{m}^2\mathrm{K/W}$.

suspension. The thermal conductivity of an iron suspension containing such field-induced percolation paths has been modeled by a two-level approach, using the Bruggeman model within the chains and Fricke/Nan effective medium theory for the overall suspension [21]. This type of model could potentially be extended to carbon nanotube suspensions, where interfacial resistance between nanotubes, and at the nanotube-liquid interface, may become significant. Percolation can *effectively* increase the length of the dispersed phase, which may result in heat-transfer augmentation in suspensions despite the increased interfacial resistance for nanoscale particles.

References

[1] Xie, H., Wang, J., Xi, T., Liu, Y., and Ai, F., 2002, "Thermal conductivity of suspension containing SiC particles," J. Mater. Sci. Lett., **21**(3), pp. 193–95.

[2] Eastman, J. A., Choi, S. U. S., Li, S., Yu, W., and Thompson, L. J., 2001, "Anomalously increased effective thermal conductivities of ethylene glycol-based nanofluids containing copper nanoparticles," Appl. Phys. Lett., **78**(6), pp. 718–720.

[3] Patel, H. E., Das, S. K., Sundararajan, T., Sreekumaran, N. A., George, B., and Pradeep, T., 2003, "Thermal conductivities of naked and monolayer protected metal nanoparticle based nanofluids: Manifestation of anomalous enhancement and chemical effects," Appl. Phys. Lett., **83**(14), pp. 2931–2933.

[4] Xie, H., Wang, J., Xi, T., Liu, Y., Ai, F., and Wu, Q., 2002, "Thermal conductivity enhancement of suspensions containing nanosized alumina particles," J. Appl. Phys., **91**(7), pp. 4568–4672.

[5] Xie, H., Wang, J., Xi, T., Liu, Y., and Ai, F., 2002, "Dependence of the thermal conductivity of nanoparticle-fluid mixture on the base fluid," J. Mater. Sci. Lett., **21**(19), pp. 1469–1471.

[6] Das, S. K., Putra, N., Thiesen, P., and Roetzel, W., 2003, "Temperature dependence of thermal conductivity enhancement for nanofluids," J. Heat Transf., **125**, pp. 567–574.

[7] Lee, S., Choi, S., Li, S., and Eastman, J. A., 1999, "Measuring thermal conductivity of fluids containing oxide nanoparticles," J. Heat Transf., **121**(2), pp. 280–289.

[8] Choi, S. U. S., Zhang, Z. G., Yu, W., and Grulke, E. A., 2001, "Anomalous thermal conductivity enhancement in nanotube suspensions," Appl. Phys. Lett., **79**(14), p. 2252.

[9] Yang, Y., Grulke, E. A., Zhang, Z. G., and Wu, G., 2006, "Thermal and rheological properties of carbon nanotube-in-oil dispersions," J. Appl. Phys., **99**(11), p. 114307.

[10] Nan, C.-W., Birringer, R., Clarke, D. R., and Gleiter, H., 1997, "Effective thermal conductivity of particulate composites with interfacial thermal resistance," J. Appl. Phys., **81**(10), pp. 6692–6699.

[11] Xue, Q. Z., 2006, "Model for the effective thermal conductivity of carbon nanotube composites," Nanotechnology, **17**(6), pp. 1655–1660.

[12] Prasher, R., Bhattacharya, P., and Phelan, P. E., 2005, "Thermal conductivity of nanoscale colloidal solutions (nanofluids)," Phys. Rev. Lett., **94**(2), p. 025901.

[13] Nan, C.-W., Liu, G., Lin, Y., and Li, M., 2004, "Interface effect on thermal conductivity of carbon nanotube composites," Appl. Phys. Lett., **85**(16), pp. 3549–3551.

[14] Zhou, X. F. and Gao, L., 2006, "Effective thermal conductivity in nanofluids of nonspherical particles with interfacial thermal resistance: Differential effective medium theory," J. Appl. Phys., **100**, p. 024913.

[15] Maxwell, J. C., 1954, *A Treatise on Electricity and Magnetism*, Dover Publications, Inc.

[16] Landau, L. D., Pitaevskii, L. P., and Lifshitz, E. M., 1984, *Electrodynamics of Continuous Media, Second Edition: Volume 8 (Course of Theoretical Physics)*, Butterworth-Heinemann.

[17] Heine, M. C., Vicente, J., and Klingenberg, D. J., 2006, "Thermal transport in sheared electro- and magnetoreological fluids," Phys. Fluids, **18**.

[18] Schueler, R., Petermann, J., Schulte, K., and Wentzel, H. P., 1998, "Agglomeration and electrical percolation behavior of carbon black dispersed in epoxy resin," J. Appl. Polym. Sci., **63**(13), pp. 1741–1746.

[19] Fricke, H., 1924, "A mathematical treatment of the electric conductivity and capacity of disperse systems," Phys. Rev., **24**(5), pp. 575–587.

[20] Bruggeman, D., 1935, "Dielectric constant and conductivity of mixtures of isotropic materials," Ann. Phys., **24**, pp. 636–664.

[21] Reinecke, B. N., Shan, J. W., Suabedissen, K. K., and Cherkasova, A. S., 2008, "On the anisotropic thermal conductivity of magnetorheological suspensions," J Appl. Phys., **104**, p. 023507.

[22] Kapitza, P. L., 1941, "Heat transfer and superfluidity of helium II," Phys. Rev., **60**, pp. 354–355.

[23] Every, A. G., Tzou, Y., Hasselman, D. P. H., and Raj, R., 1992, "The effect of particle size on the thermal conductivity of ZnS/diamond composites," Acta Metall., **40**(1), pp. 123–129.

[24] Yang, B. and Han, Z. H., 2006, "Temperature-dependent thermal conductivity of nanorod-based nanofluids," Appl. Phys. Lett., **89**(8), p. 083111.

[25] Kreith, F. and Goswami, D. Y., eds., 2005, *The CRC Handbook of Mechanical Engineering*, CRC Press.

[26] Larson, R. G., 1999, *The Structure and Rheology of Complex Fluids*, Oxford University Press.

[27] Murphy, R., Nicolosi, V., Hernandez, Y., McCarthy, D., Rickard, D., Vrbanic, D., Mrzel, A., Mihailovic, D., Blau, W. J., and Coleman, J. N., 2006, "Observation of extremely low percolation threshold in $Mo_6S_{4.5}I_{4.5}$ nanowire/polymer composites," Scripta Mater., **54**, pp. 417–420.

[28] Vadasz, J. J., Govender, S., and Vadasz, P., 2005, "Heat transfer enhancement in nano-fluids suspensions: Possible mechanisms and explanations," Int. J. Heat Mass Transf., **48**(13), pp. 2673–2683.

[29] Li, C. H., Williams, W., Buongiorno, J., Hu, L.-W., and Peterson, G. P., 2008, "Transient and steady-state experimental comparison study of effective thermal conductivity of Al_2O_3/water nanofluids," ASME J. Heat Transfer, **130**(4), p. 042407.

[30] Louge, M. and Chen, X., 2008, "Heat transfer enhancement in suspensions of agitated solids. part III: Thermophoretic transport of nanoparticles in the diffusion limit," Int. J. Heat Mass Transfer, **51**(21–22), pp. 5130–5143.

[31] Slack, G. A., 1964, "Thermal conductivity of pure and impure silicon, silicon carbide and diamond," J. Appl. Phys., **35**(12), pp. 3460–3466.

[32] Morelli, D., Heremans, J., Beetz, C., Woo, W. S., Harris, G., and Taylor, C., 1993, "Carrier concentration dependence of the thermal conductivity of silicon carbide," *Proceedings of the 5th Silicon Carbide and Related Materials Conference*, pp. 313–315.

[33] Choi, S. R., Kim, D., Choa, S.-H., Lee, S.-H., and Kim, H.-K., 2006, "Thermal conductivity of AlN and SiC thin films," Int. J. Thermophys., **27**(3), pp. 896–905.

[34] Henager, C. H. and Pawlewicz, W., 1993, "Thermal conductivities of thin, sputtered optical films," Appl. Opt., **32**, pp. 91–101.

[35] Goldberg, Y., Levinshtein, M., and Rumyantsev, S., 2001, *Silicon Carbide*, John Wiley and Sons, pp. 93–147.

[36] Kim, P., Shi, L., Majumdar, A., and McEuen, P. L., 2001, "Thermal transport measurements of individual multiwalled nanotubes," Phys. Rev. Lett., **87**(21), p. 215502.

[37] Small, J. P., Shi, L., and Kim, P., 2003, "Mesoscopic thermal and thermoelectric measurements of individual carbon nanotubes," Solid State Commun., **127**, pp. 181–186.

[38] Prasher, R., 2008, "Thermal boundary resistance and thermal conductivity of multiwalled carbon nanotubes," Phys. Rev. B, **77**, p. 075424.

[39] Li, Q., Liu, C., Wang, X., and Fan, S., 2009, "Measuring the thermal conductivity of individual carbon nanotubes by the Raman shift method," Nanotechnology, **20**, p. 145702.

[40] Fujii, M., Zhang, X., and Takahashi, K., 2006, "Measurements of thermal conductivity of individual carbon nanotubes," Phys. Status Solidi B, **243**(13), pp. 3385–3389.

[41] Choi, T.-Y., Poulikakos, D., Tharian, J., and Sennhauser, U., 2005, "Measurement of thermal conductivity of individual multiwalled carbon nanotubes by the 3-ω method," Appl. Phys. Lett., **87**, p. 013108.

[42] Choi, T.-Y., Poulikakos, D., Tharian, J., and Sennhauser, U., 2006, "Measurement of the thermal conductivity of individual carbon nanotubes by the four-point three-ω method," Nano Lett., **6**(8), pp. 1589–1593.

[43] Shioya, H., Iwai, T., Kondo, D., Nihei, M., and Awano, Y., 2007, "Evaluation of thermal conductivity of a multi-walled carbon nanotube using the Delta V-gs method," Japan. J. Appl. Phys. Part 1, **46**(5A), pp. 3139–3143.

[44] Yang, D. J., Wang, S. G., Zhang, Q., Sellin, P. J., and Chen, G., 2004, "Thermal and electrical transport in multi-walled carbon nanotubes," Phys. Lett. A, **329**(3), pp. 207–213.

[45] Che, J., Cagun, T., and Goddard, W. A. I., 2000, "Thermal conductivity of carbon nanotubes," Nanotechnology, **11**(2), pp. 65–69.

[46] Shenogin, S., Xue, L., Ozisik, R., Keblinski, P., and Cahill, D. G., 2004, "Role of thermal boundary resistance on the heat flow in carbon-nanotube composites," J. Appl. Phys., **95**(12), pp. 8136–8144.

[47] Huxtable, S., Cahill, D., Shenogin, S., Xue, L., Ozisik, R., Barone, P., Usrey, M., Strano, M., Siddons, G., Shim, M., and Keblinski, P., 2003, "Interfacial heat flow in carbon nanotube suspensions," Nature Mater., **2**, pp. 731–734.

[48] Plech, A., Kotaidis, V., Gresillon, S., Dahmen, C., and von Plessen, G., 2004, "Laser-induced heating and melting of gold nanoparticles studied by time-resolved X-ray scattering," Phys. Rev. B, **70**, pp. 195423–1–195423–7.

[49] Wilson, M. W., Hu, X., Cahill, D. G., and Braun, P. V., 2002, "Colloidal metal particles as probes of nanoscale thermal transport in fluids," Phys. Rev. B, **66**(22), p. 224301.

[50] Xue, L., Keblinski, P., Phillpot, S. R., Choi, S. U. S., and Eastman, J., 2003, "Two regimes of thermal resistance at a liquid-solid interface," J. Chem. Phys., **118**(1), pp. 337–339.

[51] Islam, M. F., Rojas, E., Bergey, D. M., Johnson, A. T., and Yodh, A. G., 2003, "High weight fraction surfactant solubilization of single-wall carbon nanotubes in water," Nano Lett., **3**(2), pp. 269–273.

[52] Wang, S., Liang, R., Wan, B., and Zhang, C., 2009, "Dispersion and thermal conductivity of carbon nanotube composites," Carbon, **47**, pp. 53–57.

[53] Snead, L. L., Nozawa, T., Katoh, Y., Byun, T.-S., Kondo, S., and Petti, D. A., 2007, "Handbook of SiC properties for fuel performance modeling," J. Nucl. Mater., **371**(1–3), pp. 329–377.

[54] Duggal, R. and Pasquali, M., 2006, "Dynamics of individual single-walled carbon nanotubes in water by real-time visualization," Phys. Rev. Lett., **96**(24), p. 246104.

[55] Ajayan, P. M. and Tour, J. M., 2007, "Nanotube composites," Nature, **447**, pp. 1066–1068.

[56] Lee, H. S. and Yun, C. H., 2008, "Translational and rotational diffusions of multi-walled carbon nanotubes with static bending," J. Phys. Chem. C, **112**, pp. 10653–10658.

[57] Arroyo, M. and Belytschko, T., 2003, "A finite deformation membrane based on inter-atomic potentials for the transverse mechanics of nanotubes," Mech. Mater., **35**(3–6), pp. 193–215.

[58] Abels, J. A., Moreno-Herrero, F., van der Heijden, T., Dekker, C., and Dekker, N. H., 2005, "Single-molecule measurements of the persistence length of double-stranded RNA," Biophys. J., **88**, pp. 2737–2744.

[59] Jang, S. and Choi, S., 2004, "Role of Brownian motion in the enhanced thermal conductivity," App. Phys. Lett., **84**, pp. 4316–4318.

[60] Evans, W., Fish, J., and Keblinski, P., 2006, "Role of brownian motion hydrodynamics on nanofluid thermal conductivity," Appl. Phy. Lett., **88**, p. 093116.

[61] Wang, Z., Tang, D. W., Li, X. B., Zheng, X. H., Zhang, W., Zheng, L. X., Zhu, Y. T., Jin, A. Z., Yang, H. F., , and Gu, C. Z., 2007, "Length-dependent thermal conductivity of an individual single-wall carbon nanotube," Appl. Phys. Lett., **91**, p. 123119.

[62] Russel, W. B., Saville, D. A., and Schowalter, W. R., 1972, *Colloidal Dispersions*, Cambridge University Press.

[63] Dobias, B., Qiu, X., and Rybinski, W., eds., 1999, *Solid - Liquid Dispersions*, CRC.

[64] Gaydardzhiev, S. and Ay, P., 2006, "Characterisation of aqueous suspensions of fumed aluminum oxide in presence of two dolapix dispersants," J. Mater. Sci., **41**, pp. 5257–5262.

[65] Li, X., Zhu, D., and Wang, X., 2007, "Evaluation of dispersion behavior of the aqueous copper nano-suspensions," J. Colloid. Interf. Sci., **310**, pp. 456–463.

[66] Singh, B., Menchavez, R., Takai, C., Fuji, M., and Takanashi, M., 2005, "Stability of dispersions of colloidal alumina particles in aqueous suspensions," J. Colloid. Interf. Sci., **291**, pp. 181–186.

[67] Ridaoui, H., Jada, A., Vidal, L., and Donnet, J.-B., 2006, "Effect of cationic surfactant and block copolymer on carbon black particle surface charge and size," Colloid. Surface. A, **278**, pp. 149–159.

[68] Hu, H., Yu, A., Kim, E., Zhao, B., Itkins, M., Bekyarova, E., and Haddon, R., 2005, "Influence of the zeta potential on the dispersability and purification of single-walled carbon nanotubes," J. Phys. Chem. B, **109**, pp. 11520–11524.

[69] Assael, M. J., Chen, C.-F., Metaxa, I., and Wakeham, W. A., 2004, "Thermal conductivity of suspensions of carbon nanotubes in water," Int. J. Thermophys., **25**(4), pp. 971–985.

[70] Esumib, K., Ishigamib, M., Nakajimab, A., Sawadab, K., and Hondab, H., 279-281, "Chemical treatment of carbon nanotubes," Carbon, **34**(2), p. 1996.

[71] Jiang, L. Q. and Gao, L., 2003, "Effect of chemical treatment on the dispersion properties of carbon nanotubes," J. Inorg. Mater., **18**(5), pp. 1135–1138.

[72] Meuer, S., Braun, L., Schilling, T., and Zentel, R., 2009, "Alpha-pyrene polymer functionalized multiwalled carbon nanotubes: Solubility, stability and depletion phenomena," Polymer, **50**(1), pp. 154–160.

[73] Edri, E. and Regev, O., 2008, "pH effects on BSA-dispersed carbon nanotubes studied by spectroscopy-enhanced composition evaluation techniques," Anal. Chem., **80**(11), pp. 4049–4054.

[74] Wang, X. J., Li, X. F., and Yang, S., 2009, "Influence of pH and SDBS on the stability and thermal conductivity of nanofluids," Energ. Fuel, **23**, pp. 2684–2689.

[75] Segota, S., Heimer, S., and Tezak, D., 2006, "New catanionic mixtures of dodecyldimethylammonium bromide/sodium dodecylbenzenesulphonate/water I. surface properties of dispersed particles," Colloid. Surface A, **274**, pp. 91–99.

[76] Mishra, S., Kanungo, S., and Rajeev, 2003, "Adsorption of sodium dodecyl benzenesulfonate onto coal," J. Colloid. Interf. Sci., **267**, pp. 42–48.

[77] Kaler, E. W., Herrington, K. L., Murthy, A. K., and Zasadzinski, J. A. N., 1992, "Phase behavior and structures of mlxtures of anionic and cationic surfactants," J. Phys. Chem., **96**, pp. 6698–6707.

[78] Tadros, T. F., 2005, *Applied surfactants: principles and application*, Willey-VCH.

[79] Ingle, J. D. J. and Crouch, S. R., 1988, *Spectrochemical Analysis*, Englewood Cliffs, N.J.: Prentice Hall.

[80] Zhang, Z.-B., Cardenas, J., Campbell, E. E. B., and Zhang, S.-L., 2005, "Reversible surface functionalization of carbon nanotubes for fabrication of field-effect transistors," Appl. Phys. Lett., **87**, p. 043110.

[81] Eda, G., Fanchini, G., Kanwal, A., and Chhowalla, M., 2008, "Bundling dynamics of single walled carbon nanotubes in aqueous suspensions," J. Appl. Phys., **103**(9), p. 093118.

[82] Mason, M. and Weaver, W., 1924, "The settling of small particles in a fluid," Phys. Rev., **23**, pp. 412–426.

[83] Hobbie, E. K., Wang, H., Kim, H., Han, C. C., Grulke, E. A., and Obrzut, J., 2003, "Optical measurements of structure and orientation in sheared carbon-nanotube suspensions," Rev. Sci. Instrum., **74**(3), pp. 1244–1250.

[84] Bubke, K., Gnewuch, H., Hempstead, M., Hammer, J., and Green, M. L. H., 1997, "Optical anisotropy of dispersed carbon nanotubes induced by electric field," Appl. Phys. Lett., **71**(14), pp. 1906–1908.

[85] Lin, C. and Shan, J., 2007, "Electrically tunable viscosity of dilute suspensions of carbon nanotubes," Phys. Fluid., **19**, p. 121702.

[86] Brown, J. W., M. S. and. Shan, Lin, C., and Zimmermann, F. M., 2007, "Electrical polarizability of carbon nanotubes in liquid suspension," Appl. Phys. Lett., **90**, p. 203108.

[87] Korneva, G., Ye, H., Gogotsi, Y., Halverson, D., Friedman, G., Bradley, J.-C., and Kornev, K. G., 2005, "Carbon nanotubes loaded with magnetic particles," Nano Lett., **5**(5), pp. 879–884.

[88] Walters, D. A., Casavant, M. J., Qin, X. C., Huffman, C. B., Boul, P. J., Ericson, L. M., Haroz, E. H., O'Connell, M. J., Smith, K., Colbert, D. T., and Smalley, R. E., 2001, "In-plane-aligned membranes of carbon nanotubes," Chem. Phys. Lett., **338**(1), pp. 14–20.

[89] Hone, J., Llaguno, M. C., Nemes, N. M., Johnson, A. T., Fischer, J. E., Walters, D. A., Casavant, M. J., Schmidt, J., and Smalley, R. E., 2000, "Electrical and thermal transport properties of magnetically aligned single walt carbon nanotube films," Appl. Phys. Lett., **77**(15), pp. 666–668.

Vita

Anna S. Cherkasova

2009	Ph.D. in Mechanical and Aerospace Engineering from Rutgers, the State University of New Jersey
2000-2002	M.Sc. in Physics and Applied Mathematics from Moscow Institute of Physics and Technology
1996-2000	B.Sc. in Physics and Applied Mathematics from Moscow Institute of Physics and Technology
2005-2009	Graduate assistant, Department of Mechanical and Aerospace Engineering, Rutgers, the State University of New Jersey
2004-2005	Teaching assistant, Department of Mechanical and Aerospace Engineering, Rutgers, Rutgers, the State University of New Jersey